Assessment of the $RE(OH)_3$ Ising magnetic materials as possible candidates for the study of transverse-field-induced quantum phase transitions

Pawel Stasiak[1] and Michel J. P. Gingras[1,2,3]

[1]*Department of Physics and Astronomy, University of Waterloo, Waterloo, Ontario, Canada N2L-3G1*

[2]*Department of Physics and Astronomy, University of Canterbury, Private Bag, 4800 Christchurch, New Zealand*

[3]*Canadian Institute for Advanced Research, 180 Dundas St. W., Toronto, Ontario, Canada M5G 1Z8*

(Received 21 December 2006; published 12 December 2008)

The $LiHo_xY_{1-x}F_4$ Ising magnetic material subject to a magnetic field perpendicular to the Ho^{3+} Ising direction has shown over the past 20 years to be a host of very interesting thermodynamic and magnetic phenomena. Unfortunately, the availability of other magnetic materials other than $LiHo_xY_{1-x}F_4$ that may be described by a transverse-field Ising model remains very much limited. It is in this context that we use here a mean-field theory to investigate the suitability of the $Ho(OH)_3$, $Dy(OH)_3$, and $Tb(OH)_3$ insulating hexagonal dipolar Ising-type ferromagnets for the study of the quantum phase transition induced by a magnetic field, B_x, applied perpendicular to the Ising spin direction. Experimentally, the zero-field critical (Curie) temperatures are known to be $T_c \approx 2.54$, 3.48, and 3.72 K, for $Ho(OH)_3$, $Dy(OH)_3$, and $Tb(OH)_3$, respectively. From our calculations we estimate the critical transverse field, B_x^c, to destroy ferromagnetic order at zero temperature to be $B_x^c = 4.35$, 5.03, and 54.81 T for $Ho(OH)_3$, $Dy(OH)_3$, and $Tb(OH)_3$, respectively. We find that $Ho(OH)_3$, similarly to $LiHoF_4$, can be quantitatively described by an effective $S=1/2$ transverse-field Ising model. This is not the case for $Dy(OH)_3$ due to the strong admixing between the ground doublet and first excited doublet induced by the dipolar interactions. Furthermore, we find that the paramagnetic (PM) to ferromagnetic (FM) transition in $Dy(OH)_3$ becomes first order for strong B_x and low temperatures. Hence, the PM to FM zero-temperature transition in $Dy(OH)_3$ may be first order and not quantum critical. We investigate the effect of competing antiferromagnetic nearest-neighbor exchange and applied magnetic field, B_z, along the Ising spin direction $\hat{z}$ on the first-order transition in $Dy(OH)_3$. We conclude from these preliminary calculations that $Ho(OH)_3$ and $Dy(OH)_3$ and their Y^{3+} diamagnetically diluted variants, $Ho_xY_{1-x}(OH)_3$ and $Dy_xY_{1-x}(OH)_3$, are potentially interesting systems to study transverse-field-induced quantum fluctuations effects in hard axis (Ising-type) magnetic materials.

DOI: 10.1103/PhysRevB.78.224412 PACS number(s): 75.30.Kz, 75.50.−y, 75.40.Cx, 73.43.Nq

I. INTRODUCTION

A. Transverse-field Ising model

Quantum phase transitions occur near zero temperature and are driven by quantum-mechanical fluctuations associated with the Heisenberg uncertainty principle and not by thermal fluctuations as in the case of classical temperature-driven phase transitions.[1,2] There is accumulating evidence that the exotic behavior exhibited by several metallic, magnetic, and superconducting materials may have its origin in underlying large quantum fluctuations and proximity to a quantum phase transition. For this reason, much effort is currently being devoted to understand quantum phase transitions in a wide variety of condensed-matter systems.

Perhaps the simplest model that embodies the phenomenon of a quantum phase transition is the transverse-field Ising model (TFIM),[3,4] first proposed by de Gennes[5] to describe proton tunneling in ferroelectric materials. The spin Hamiltonian for the TFIM reads

$$H_{\mathrm{TFIM}} = -\frac{1}{2}\sum_{(\boldsymbol{r}_i,\boldsymbol{r}_j)} J_{ij}[|\boldsymbol{r}_j - \boldsymbol{r}_i|]S_i^z(\boldsymbol{r}_i)S_j^z(\boldsymbol{r}_j) - \Gamma\sum_{(\boldsymbol{r}_i)} S_i^x(\boldsymbol{r}_i). \quad (1)$$

The $\boldsymbol{S}_i$ ($S=1/2$) quantum spin operators reside on the lattice sites, $\boldsymbol{r}_i$, of some d-dimensional lattice. The $\boldsymbol{S}_i$ operators are related to the Pauli spin matrices by $\boldsymbol{S}_i = \frac{1}{2}\boldsymbol{\sigma}_i$. (Here we set $\hbar = 1$.) The components of $\boldsymbol{S}_i$ obey the commutation relations $[S_i^\alpha, S_j^\beta] = i\epsilon_{\alpha\beta\gamma}S_i^\gamma\delta_{ij}$, where α, β, and γ indicate x, y, or z spin components, and δ_{ij} and $\epsilon_{\alpha\beta\gamma}$ are the Kronecker delta and fully antisymmetric Levi-Cevita tensor, respectively. Γ is the effective transverse field along the x direction, perpendicular to the Ising z axis. As described below, Γ does not correspond onto to one to the real applied physical transverse field, B_x. Rather, Γ in Eq. (2) is a function of B_x. In fact, J_{ij} is also a function of B_x.[6–8] If the spin interactions, J_{ij}, possess translational invariance, the system displays for $\Gamma = 0$ conventional long-range magnetic order below some critical temperature, T_c. In the simplest scenario, where $J_{ij} > 0$, the ordered phase is ferromagnetic (FM) and the order parameter is the average magnetization per spin, $m_z = (1/N)\Sigma_i\langle S_i^z\rangle$, where N is the number of spins. Since S_i^x and S_i^z do not commute, nonzero Γ causes quantum tunneling between the spin-up, $|\uparrow\rangle$, and spin-down, $|\downarrow\rangle$, eigenstates of S_i^z. By increasing Γ, T_c decreases until, ultimately, $T_c(\Gamma)$ vanishes at a *quantum critical point* where $\Gamma = \Gamma_c$. On the $T=0$ temperature axis, the system is in a long-range ordered phase for $\Gamma < \Gamma_c$, while it is in a quantum paramagnetic (PM) phase for $\Gamma > \Gamma_c$. The phase transition between the paramagnetic and long-range ordered phase at Γ_c constitutes the quantum phase transition.[3,4]

One can also consider generalizations of the H_{TFIM} where the J_{ij} are quenched (frozen) random interactions. Of particular interest is the situation where there are as many ferromagnetic $J_{ij} > 0$ and antiferromagnetic $J_{ij} < 0$ couplings. This

causes a high level of random frustration, and the system, provided it is three dimensional, freezes into a spin-glass (SG) state via a true thermodynamic phase transition at a spin-glass critical temperature T_g.[9,10] Here as well, one can investigate how the spin-glass transition is affected by a transverse field Γ. As in the previous example, $T_g(\Gamma)$ decreases as Γ is increased from zero until, at $\Gamma=\Gamma_c$, a quantum phase transition between a quantum paramagnet and a spin-glass phase ensues. Extensive numerical studies have found the quantum phase transition between a quantum paramagnet and a spin-glass phase[11–13] to be quite interesting due to the occurrence of Griffiths-McCoy singularities (GMS).[14,15] These GMS arise from rare spatial regions of disorder which may, for example, resemble the otherwise nonrandom (disorder-free) version of the system at stake. As a result, GMS can lead to singularities in various thermodynamic quantities away from the quantum critical point.

B. $LiHo_xY_{1-x}F_4$

On the experimental side, most studies aiming at exploring the phenomena associated with the TFIM have focused on the insulating $LiHo_xY_{1-x}F_4$ Ising magnetic material.[16–32] In this system, the Ho^{3+} Ising spin direction is parallel to the c axis of the body-centered tetragonal structure of $LiHo_xY_{1-x}F_4$. The random disorder is introduced by diluting the magnetic Ho^{3+} ions by nonmagnetic Y^{3+}. Crystal-field effects lift the degeneracy of the $^5I_8$ electronic manifold, giving an Ising ground doublet, $|\Phi_0^{\pm}\rangle$, and a first excited singlet, $|\Phi_e\rangle$, at approximately 11 K above the ground doublet.[26] The remaining 14 crystal-field states lie at much higher energies.[26] Quantum spin-flip fluctuations are introduced by the application of a magnetic field, B_x, perpendicular to the Ising c axis. B_x admixes $|\Phi_e\rangle$ with $|\Phi_0^{\pm}\rangle$, splitting the latter states and producing an effective TFIM with $\Gamma(B_x)\propto B_x^2$ for small B_x.[6–8]

The properties of pure $LiHoF_4$ in a transverse B_x are now generally qualitatively well understood.[6,7] Indeed, a recent quantum Monte Carlo study[6] found general agreement between experiments and a microscopic model of $LiHoF_4$. However, some quantitative discrepancies between Monte Carlo and experimental data, even near the classical paramagnetic to ferromagnetic transition where B_x/T_c is small, do exist.[6,7] One noteworthy effect at play in $LiHo_xY_{1-x}F_4$ at low temperatures is the significant enhancement of the zero-temperature critical B_x, B_x^c, caused by strong hyperfine nuclear interactions in Ho^{3+}-based materials.[6,20,25,26,33]

$LiHo_xY_{1-x}F_4$ in a transverse B_x and $x<1$ has long been known to display paradoxical behaviors both in the FM ($0.25<x<1.0$) and SG ($x<0.25$) regimes. In the FM regime, a mean-field behavior, $T_c(x)\propto x$, for the PM to FM transition is observed when $B_x=0$.[21,22] However, in nonzero B_x, the rate at which $T_c(B_x)$ is reduced by $B_x>0$ increases faster than what mean-field theory (MFT) predicts as x is reduced.[22,27] In the high Ho^{3+} (SG) dilution regime (e.g., $LiHo_{0.167}Y_{0.833}F_4$), $LiHo_xY_{1-x}F_4$ has long been[17–19,30,32] argued to display a conventional SG transition for $B_x=0$ signaled by a nonlinear magnetic susceptibility, χ_3, diverging at T_g as $\chi_3(T)\propto(T-T_g)^{-\gamma}$.[10] However, $\chi_3(T)$ becomes less singular as B_x is increased from $B_x=0$, suggesting that no quantum phase transition between a PM and a SG states exists as $T\to 0$.[18,19] Recent theoretical studies[8,34,35] suggest that for dipole-coupled Ho^{3+} in a diluted sample, nonzero B_x generates longitudinal (along the Ising $\hat{z}$ direction) random fields that (i) lead to a faster decrease in $T_c(B_x)$ in the FM regime[22,27,35] and (ii) destroy the PM to SG transition for samples that otherwise show a SG transition when $B_x=0$,[8,18,19,29,31,32,34,35] or, at least, lead to a disappearance of the χ_3 divergence as B_x is increased from zero.[18,19,35]

Perhaps the most interesting among the phenomena exhibited by $LiHo_xY_{1-x}F_4$ is the one referred to as *antiglass* and which has been predominantly investigated in $LiHo_{0.045}Y_{0.955}F_4$.[16,23,24,29,36–38] The reason for this name comes from ac susceptibility data on $LiHo_{0.045}Y_{0.955}F_4$ which show that the distribution of relaxation times *narrows* upon cooling below 300 mK.[16,23,24] This behavior is quite different from that observed in conventional spin glasses where the distribution of relaxation times broadens upon approaching a spin-glass transition at $T_g>0$.[9,10] The antiglass behavior has been interpreted as evidence that the spin-glass transition in $LiHo_xY_{1-x}F_4$ disappears at some nonzero $x_c>0$. Results from more recent experimental studies on $LiHo_{0.165}Y_{0.835}F_4$ ($x=16.5\%$) and $LiHo_{0.045}Y_{0.955}F_4$ ($x=4.5\%$) suggest an absence of a genuine spin-glass transition even for a concentration of Ho as large as 16.5%.[29,32] In particular, it is in stark contrast with theoretical arguments[39] which predict that because of the long-ranged $1/r^3$ nature of dipolar interactions, classical dipolar Ising spin glasses should have $T_g(x)>0$ for all $x>0$. However, very recent work asserts that there is indeed a thermodynamic SG transition for $x=16.5\%$ (Ref. 30) but that the behavior found in $LiHo_{0.045}Y_{0.955}F_4$ is truly unconventional.[30,36–38]

Two very different scenarios for the failure of $LiHo_{0.045}Y_{0.955}F_4$ to show a spin-glass transition have been put forward.[24,40–42] First, it has been suggested that the (small) off-diagonal part of the dipolar interactions leads to virtual crystal-field excitations that admix $|\Phi_0^{\pm}\rangle$ with $|\Phi_e\rangle$ and give rise to nonmagnetic singlets for spatially close pairs of Ho^{3+} ions.[24] The formation of these singlets would thwart the development of a spin-glass state. This mechanism is analogous to the one leading to the formation of the random singlet state in dilute antiferromagnetically coupled $S=1/2$ Heisenberg spins.[43] However, a recent study[44] shows that the energy scale for this singlet formation is very low ($\sim 10^0$ mK) and that the random singlet mechanism[24] may not be very effective at destroying the spin-glass state in $LiHo_{0.045}Y_{0.955}F_4$. Hence the proposed formation of an entangled state in $LiHo_{0.045}Y_{0.955}F_4$ may, if it really exist, perhaps proceed via a more complex scheme than that proposed in Ref. 24. Also, the low-temperature features observed in the specific heat in Ref. 24 have not been observed in a more recent study.[36] Second and from a completely different perspective, numerical simulations of *classical* Ising dipoles found that the spin-glass transition temperature, T_g, appears to vanish for a concentration of dipoles below approximately 20% of the sites occupied.[40–42] However, even more recent Monte Carlo simulations find that this conclusion may not be that firmly established.[45]

As another possible and yet unexplored scenario, we note here that since Ho^{3+} is an even electron system (i.e., a non-

Kramers ion), Kramers' theorem is inoperative and the ground-state doublet can be split by random (electrostatic) crystal-field effects that compete with the collective spin-glass behavior. For example, random strains, which may come from the substitution of $Ho^{3+} \rightarrow Y^{3+}$, break the local tetragonal symmetry and introduces (random) crystal-field operators (e.g., $O_2^{\pm 2}$) which have nonzero matrix elements between the two states, $|\Phi_0^+\rangle$ and $|\Phi_0^-\rangle$, of the ground doublet, splitting it, and possibly destroying the spin-glass phase at low Ho^{3+} concentration. Indeed, such random transverse fields have been identified in samples with very dilute Ho^{3+} in a $LiYF_4$ matrix.[46,47] Also, very weak random strains, hence effective random transverse fields, arise from the different (random) anharmonic zero-point motions of ^6Li and ^7Li in $Ho:LiYF_4$ samples with natural abundance of ^6Li and ^7Li.[48] Finally, there may be intrinsic strains in the crystalline samples that do not arise from the Ho^{3+}/Y^{3+} or $^6Li/^7Li$ admixture.[46] However, using available estimates,[46–48] calculations suggests that strain-induced random fields at play in $LiHo_{0.045}Y_{0.955}F_4$ may be too small [$<O(10^1$ mK)] to cause the destruction of the spin-glass phase in this system.[49] Nevertheless, the point remains that, in principle, the non-Kramers nature of Ho^{3+} does offer a route for the destruction of the spin-glass phase in $LiHo_xY_{1-x}F_4$ outside strictly pairwise, quantum,[24,44] or classical[40–42,45] magnetic interaction mechanisms. At this stage, this is clearly a matter that needs to be investigated experimentally further. One notes that because of Kramers' theorem, the destruction of a SG phase via strain-induced effective random transverse fields would not occur for an odd-electron (Kramers) ion such as Dy^{3+} or Er^{3+}. In that context, one might think that a comparison of the behavior of $LiDy_xY_{1-x}F_4$ or $LiEr_xY_{1-x}F_4$ with that of $LiHo_xY_{1-x}F_4$ would be interesting. Unfortunately, while $LiHo_xY_{1-x}F_4$ is an Ising system, the Er^{3+} and Dy^{3+} moments in $LiEr_xY_{1-x}F_4$ and $LiDy_xY_{1-x}F_4$ are *XY*-like.[50,51] Hence, one cannot compare the $LiEr_xY_{1-x}F_4$ and $LiDy_xY_{1-x}F_4$ *XY* compounds with the $LiHo_xY_{1-x}F_4$ Ising material on the same footing.

From the above discussion, it is clear that there are number of fundamental questions raised by experimental studies of $LiHo_xY_{1-x}F_4$ both in zero and nonzero transverse fields that warrant systematic experimental investigations in other similar diamagnetically diluted dipolar Ising-type magnetic materials. Specific questions are:

(1) How does the quantum criticality of a transverse-field Ising material with much smaller hyperfine interactions than Ho^{3+} in $LiHo_xY_{1-x}F_4$ manifest itself?[20,25,33]

(2) Is the theoretical proposal of transverse-induced random longitudinal fields in diluted dipolar Ising materials[8,34,35] valid and can it be explored and confirmed in other materials other than $LiHo_xY_{1-x}F_4$?[27] In particular, can the phenomena observed in Ref. 27 and ascribed to Griffiths singularities be observed in other disordered dipolar Ising systems subject to a transverse field?

(3) Does the antiglass phenomenon[16,23,24,38] occur in other diluted dipolar Ising materials? If yes, which, if any, of the aforementioned theoretical proposals for the destruction of the spin-glass state at small Ho^{3+} concentration is correct?

C. $RE(OH)_3$ materials

As mentioned above, these questions cannot be investigated with the $LiEr_xY_{1-x}F_4$ and $LiDy_xY_{1-x}F_4$ materials isostructural to the $LiHo_xY_{1-x}F_4$ Ising compound since they are *XY*-like systems. However, we note in passing that it would nevertheless be interesting to explore the topic of induced random fields[8,34,35] and the possible existence of a *XY* dipolar spin-glass and/or antiglass state in $LiEr_xY_{1-x}F_4$ and $LiDy_xY_{1-x}F_4$. The $LiTb_xY_{1-x}F_4$ material is of limited use in such investigations since the single-ion ground state of Tb^{3+} in this compound consists of two separated singlets[52] and local moment magnetism on the Tb^{3+} site disappears at low Tb concentration.[53] In this paper, we propose that the $RE(OH)_3$ (RE=Ho,Dy) compounds may offer themselves as an attractive class of materials to study the above questions. Similarly to the $LiHoF_4$, the $RE(OH)_3$ materials possess the following interesting properties:

(1) They are insulating rare-earth materials.

(2) Their main spin-spin couplings are magnetostatic dipole-dipole interactions.

(3) The $RE(OH)_3$ materials are stable at room temperature.

(4) Both pure $RE(OH)_3$ and $LiHoF_4$ are collinear (Ising-type) dipolar ferromagnets with the Ising direction along the *c* axis of a hexagonal unit cell [$RE(OH)_3$] or body-centered tetragonal unit cell ($LiHoF_4$). In both cases there are two magnetically equivalent ions per unit cell.

(5) In $RE(OH)_3$, the Kramers (Dy^{3+}) and non-Kramers (Ho^{3+}) variants possess a common crystalline structure and both have similar bulk magnetic properties in zero transverse magnetic field, B_x.

(6) The critical temperature of the pure $RE(OH)_3$ compounds is relatively high, ~3 K. This would make possible the study of Y-substituted Dy and Ho hydroxides down to quite low concentration of rare earth while maintaining the relevant magnetic temperature scale above the lowest attainable temperature with a commercial dilution refrigerator.

(7) Finally, and this is a key feature that motivated the present study, the first excited crystal-field state in the $Ho(OH)_3$ and $Dy(OH)_3$ compounds is low lying, hence allowing a possible transverse-field-induced admixing and, possibly, a transverse-field Ising model description.[54]

To the best of our knowledge, it appears that the $RE(OH)_3$ materials have so far not been investigated as potential realization of the TFIM. The purpose of this paper is to explore (i) the possible description of these materials as a TFIM, (ii) obtain an estimate of what the zero-temperature critical transverse field, B_x^c, may be and, (iii) assess if any new interesting phenomenology may occur, even in undiluted $RE(OH)_3$ compounds, in nonzero transverse field, B_x.

We note, however, that there are so far no very large single crystals of $RE(OH)_3$ available.[55] For example, their length typically varies between 3 and 17 mm and their diameter between 0.2 and 0.6 mm. The lack of large single crystals would make difficult neutron-scattering experiments. However, possibly motivated by this work and by a first generation of bulk measurements (e.g., susceptibility and specific heat), experimentalists and solid-state chemists may be able to conceive ways to grow larger single crystals of

TABLE I. Position parameters of O^{2-} and H^- ions in rare-earth hydroxides and $Y(OH)_3$ from Refs. 57 and 58 (see text in Sec. II A).

	O^{2-}, x	O^{2-}, y	H^-, x	H^-, y
$Tb(OH)_3$	0.3952(7)	0.3120(6)	0.276(1)	0.142(1)
$Dy(OH)_3$	0.3947(6)	0.3109(6)	0.29(3)	0.15(2)
$Ho(OH)_3$	0.3951(7)	0.3112(7)	0.30(3)	0.17(3)
$Y(OH)_3$	0.3958(6)	0.3116(6)	0.28(1)	0.17(1)

$RE(OH)_3$. Also, in light of the fact that most experiments on $LiHo_xY_{1-x}F_4$ that have revealed exotic behavior are bulk measurements,[16–18,21,23,24,36,37] we hope that at this time the lack of availability of large single crystals of the $RE(OH)_3$ series is not a strong impediment against pursuing a first generation of bulk experiments on $RE(OH)_3$.

The rest of this paper is organized as follows. In Sec. II, we review the main single-ion magnetic properties of $RE(OH)_3$ (RE=Dy,Ho,Tb). In particular, we discuss the crystal-field Hamiltonian of these materials and the dependence of the low-lying crystal-field levels on an applied transverse field, B_x. We present in Sec. III a mean-field calculation to estimate the B_x vs temperature, T, phase diagram of these materials. In Sec. IV, we show that $Ho(OH)_3$ and $Tb(OH)_3$ can be described quantitatively well by a transverse-field Ising model, while $Dy(OH)_3$ cannot. Section V A, uses a Ginzburg-Landau theory to explore the first-order PM to FM transition that occurs in $Dy(OH)_3$ at low temperatures and strong B_x. Section V B discusses the effect of nearest-neighbor antiferromagnetic exchange interaction and applied longitudinal (i.e., along the $\hat{z}$ axis) magnetic field, B_z, on the first-order transition in $Dy(OH)_3$. A brief conclusion is presented in Sec. VI. The Appendix discusses how the excited crystal-field states in $Dy(OH)_3$ play an important quantitative role on the determination of $T_c(B_x)$ in this material.

II. $RE(OH)_3$: MATERIAL PROPERTIES

A. Crystal properties

All the rare-earth hydroxides form hexagonal crystals that that are isostructural with $Y(OH)_3$. The lattice is described by translation vectors $\boldsymbol{a_1}=(0,0,0)$, $\boldsymbol{a_2}=(-a/2,a\sqrt{3}/2,0)$, and $\boldsymbol{a_3}=(0,0,c)$. A unit cell consist of two Ho^{3+} ions at coordinates (1/3,2/3,1/4) and (2/3,1/3,3/4) in the basis of lattice vectors $\boldsymbol{a_1}$, $\boldsymbol{a_2}$, and $\boldsymbol{a_3}$. The coordinates of three O^{2-} and H^- ions, relative to the position of Ho^{3+}, are $\pm(x,y,0)$, $\pm(-y,x-y,0)$, and $\pm(y-x,-x,0)$, where $\pm$ refers to the first and second Ho^{3+} in the unit cell, respectively.[56] The values of the parameters x and y for $Y(OH)_3$ are listed in Table I. The lattice structure is depicted in Fig. 1. The lattice constants for $Tb(OH)_3$, $Dy(OH)_3$, $Ho(OH)_3$, and $Y(OH)_3$ from Beall *et al.*[57] are collected in Table II. Each magnetic ion is surrounded by nine oxygen atoms that create a crystalline field characterized by the point-group symmetry C_{3h}.[56]

B. Single-ion properties

The electronic configuration of the magnetic ions Tb^{3+}, Dy^{3+}, and Ho^{3+} is, respectively, $4f^8$, $4f^9$, and $4f^{10}$. Magnetic properties of the rare-earth ions can be described by the states of the lowest-energy multiplet: the spin-obit splitting between the ground-state J manifold and the first excited states is of order of few thousand Kelvins. The ground-state manifolds can be found from Hund's rules and are $^7F_6$, $^6H_{15/2}$, and $^5I_8$ for Tb^{3+}, Dy^{3+}, and Ho^{3+}, respectively. The Wigner-Eckart theorem gives the Landé g factor equal to $\frac{3}{2}$, $\frac{4}{3}$, and $\frac{5}{4}$ for Tb^{3+}, Dy^{3+}, and Ho^{3+}, respectively.

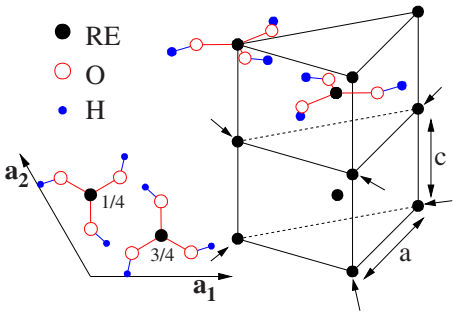

FIG. 1. (Color online) The lattice structure of rare-earth hydroxides and $Y(OH)_3$. The arrows indicate the six nearest neighbors of the central ion in the lower prism. The lower left corner shows a projection of the unit cell onto the plane given by lattice vectors $\boldsymbol{a}_1$ and $\boldsymbol{a}_2$.

In a crystalline environment, an ion is subject to the electric field and covalency effects from the surrounding ions. This crystalline field effect partially lifts the degeneracy of the ground-state multiplet. The low-energy levels of Tb^{3+} in $Tb(OH)_3$ are a pair of singlets that consist of the symmetric combination of $|\pm 6\rangle$ states with a small admixture of the $|0\rangle$ state and an antisymmetric combination 0.3 cm^{-1} above.[59] The next excited state is well separated from the lowest-energy pair by an energy of 118 cm^{-1} (Ref. 59) (1 cm^{-1} $\approx$1.44 K). In the case of Dy^{3+} in $Dy(OH)_3$, the spectrum consist of eight Kramers doublets with the first excited state 7.8 cm^{-1} above the ground state.[60] The low-energy spectrum of Ho^{3+} in $Ho(OH)_3$ is composed of a ground-state doublet and an excited singlet state 11.1 cm^{-1} above.[56]

Due to the strong shielding of the $4f$ electrons by the electrons of the filled outer electronic shells, the exchange interactions for $4f$ electrons is weak and the crystal field can be considered as a perturbation to the fixed J manifold. Furthermore, because strong spin-orbit interaction yields a large energy gap between the ground-state multiplet and the excited electronic levels, we neglect all the excited electronic multiplets in the calculation.

According to arguments provided by Stevens,[61] we express the matrix elements of the crystal-field Hamiltonian for

TABLE II. Lattice constants for rare-earth hydroxides and $Y(OH)_3$ (from Ref. 57).

	a	c	c/a
$Tb(OH)_3$	6.315(4)	3.603(2)	0.570(5)
$Dy(OH)_3$	6.286(3)	3.577(1)	0.569(0)
$Ho(OH)_3$	6.266(2)	3.553(1)	0.567(0)
$Y(OH)_3$	6.261(2)	3.544(1)	0.566(0)

TABLE III. Stevens' multiplicative factors.

Ion	α_J	β_J	γ_J
Tb^{3+}	$-1/(3^2\cdot 11)$	$2/(3^3\cdot 5\cdot 11^2)$	$-1/(3^4\cdot 7\cdot 11^2\cdot 13)$
Dy^{3+}	$-2/(3^2\cdot 5\cdot 7)$	$-2^3/(3^3\cdot 5\cdot 7\cdot 11\cdot 13)$	$2^2/(3^3\cdot 7\cdot 11^2\cdot 13^2)$
Ho^{3+}	$-1/(2\cdot 3^2\cdot 5^2)$	$-1/(2\cdot 3\cdot 5\cdot 7\cdot 11\cdot 13)$	$-5/(3^3\cdot 7\cdot 11^2\cdot 13^2)$

the ground-state manifold in terms of operator equivalents. The details of the method and conventions for expressing the crystal-field Hamiltonian can be found in the paper of Hutchings.[62] On the basis of the Wigner-Eckart theorem, one can write the crystal-field Hamiltonian in the form

$$\mathcal{H}_{\rm cf} = \sum_{nm} \theta_n B_n^m O_n^m, \tag{2}$$

where O_n^m are Stevens' "operator equivalents," θ_n are constants called Stevens' multiplicative factors, and B_n^m are crystal-field parameters (CFP). The CFP are usually determined by fitting experimental (spectroscopic) data. From angular momentum algebra, we know that in the case of f electrons, we need to consider only $n=0,2,4,6$ in the sum, Eq. (2). The choice of B_n^m coefficients in Hamiltonian (2) that do not vanish and have nonzero corresponding matrix elements is dictated by the point-symmetry group of the crystalline environment. The Stevens operators, O_n^m, are conveniently expressed in terms of vector components of the angular momentum operator, $\boldsymbol{J}$. In the case of the RE(OH)$_3$ materials considered herein, the point-symmetry group is C_{3h}, and the crystal-field Hamiltonian is of the form

$$\mathcal{H}_{\rm cf}(\boldsymbol{J}_i) = \alpha_J B_2^0 O_2^0(\boldsymbol{J}_i) + \beta_J B_4^0 O_4^0(\boldsymbol{J}_i) + \gamma_J B_6^0 O_6^0(\boldsymbol{J}_i) + \gamma_J B_6^6 O_6^6(\boldsymbol{J}_i). \tag{3}$$

The Stevens multiplicative factors α_J, β_J, and γ_J (θ_2, θ_4, and θ_6) are collected in Table III.

For the sake of conciseness and to illustrate the procedure, most of our numerical results below are presented for one set of CFP only. The qualitative picture that emerges from our calculations does not depend on the specific choice of CFP. Only quantitative differences are found using different sets of CFP. Ultimately, a further experimental determination of accurate B_n^m values would need to be carried out in order to obtain more precise mean-field estimates as well as to perform quantum Monte Carlo simulations of the Re(OH)$_3$ systems. According to our *arbitrary* choice,[63] if not stated otherwise, we use in the calculations the CFP provided by Scott *et al.*[56,59,60,64] For Ho(OH)$_3$ and Dy(OH)$_3$ different values of CFP were proposed by Karmakar *et al.*[65,66] As one can see in Fig. 3, for Ho(OH)$_3$, the latter set of CFP yields a somewhat higher mean-field critical temperature and quite a bit higher critical value of the transverse magnetic field $B_x^c=7.35$ T compared with $B_x^c=4.35$ T obtained using the CFP of Scott *et al.*[56] (see lower inset of Fig. 3). Similarly, the CFP of Karmakar *et al.*[66] for Dy(OH)$_3$ give a much higher critical field of $B_x^c=9.12$ T compared with $B_x^c=5.03$ T when the CFP of Scott *et al.*[56,60,64] are used. From the two sets of CFP for Tb(OH)$_3$ we choose the one obtained from measurements on pure Tb(OH)$_3$.[56] Using the CFP obtained for the system with a dilute concentration of Tb in a Y(OH)$_3$ matrix, Tb:Y(OH)$_3$ (Ref. 56) makes only a small change in the value of critical transverse field; we obtained $B_x^c=50.0$ and 54.8 T calculated using Tb:Y(OH)$_3$ and Tb(OH)$_3$ CFP, respectively (see upper inset of Fig. 3). Available values of the CFP are given in Table IV.

We show in Table V the lowest eigenstates and eigenvalues of the crystal-field Hamiltonian (3). The calculated energies are not in full agreement with the experimentally determined values because the CFP were fitted using all the observed optical transitions, including transitions between different $\boldsymbol{J}$ manifolds.[56] Furthermore, the fitting procedure used by Scott[56] includes perturbative admixing between manifolds with the admixing incorporated into effective Stevens' multiplicative factors α_J, β_J, and γ_J that slightly differ from those given in Table III.

Given the uncertainty in the CFP, which ultimately lead to an uncertainty of approximately ~40% on B_x^c for Ho(OH)$_3$ and Dy(OH)$_3$, as well as the nature of the mean-field calculations that we use, and which neglects thermal and quantum-mechanical fluctuations, and as well as for simplicity sake, we ignore here the effect of hyperfine coupling of the electronic and nuclear magnetic moments. However, as shown for $LiHo_xY_{1-x}F_4$, the important role of hyperfine interactions for Ho^{3+} on the precise determination of B_x^c must eventually be considered.[6,20,25,33] At this time, one must await results from further experiments and a precise set of CFP for $\mathcal{H}_{\rm cf}$ in order to go beyond the mean-field calculations presented below or to pursue quantum Monte Carlo

TABLE IV. Crystal-field parameters. Some of the calculations were performed with one set of crystal-field parameters only. Crystal-field parameters arbitrary chosen (Ref. 63) to be used in these calculations are marked with *.

Ref.	Crystal	B_2^0 (cm^{-1})	B_4^0 (cm^{-1})	B_6^0 (cm^{-1})	B_6^6 (cm^{-1})
56	Tb(OH)$_3$*	207.9 ± 2.8	-69.0 ± 1.6	-45.3 ± 1.1	585 ± 10
56	Tb:Y(OH)$_3$	189.1 ± 2.6	-69.1 ± 1.5	-45.7 ± 1.0	606 ± 9
56	Dy(OH)$_3$*	209.4 ± 3.4	-75.5 ± 3.5	-40.1 ± 1.9	541.8 ± 26.5
65	Ho(OH)$_3$	200 ± 2.0	-57 ± 0.5	-40 ± 0.5	400 ± 5
56	Ho:Y(OH)$_3$*	246.0 ± 3.4	-56.7 ± 1.2	-39.8 ± 0.3	543.6 ± 3.3
66	Dy(OH)$_3$	215.9	−72.0	−42.0	515.3

TABLE V. Eigenstates and energy levels calculated with the crystal-field parameters collected in Table IV.

Eigenstate	Energy [cm^{-1}]
$Dy(OH)_3$	
$0.92\|\pm 15/2\rangle - 0.15\|\pm 3/2\rangle + 0.37\|\mp 9/2\rangle$	
$0.40\|\pm 15/2\rangle + 0.20\|\pm 3/2\rangle - 0.90\|\mp 9/2\rangle$	9.6
$Dy(OH)_3$ [a]	
$0.98\|\pm 15/2\rangle - 0.09\|\pm 3/2\rangle + 0.15\|\mp 9/2\rangle$	
$0.17\|\pm 15/2\rangle + 0.22\|\pm 3/2\rangle - 0.96\|\mp 9/2\rangle$	19.3
$Ho{:}Y(OH)_3$	
$0.94\|\pm 7\rangle + 0.31\|\pm 1\rangle + 0.15\|\mp 5\rangle$	
$0.59\|6\rangle + 0.55\|0\rangle + 0.59\|-6\rangle$	12.7
$Ho(OH)_3$ [a]	
$0.97\|\pm 7\rangle + 0.24\|\pm 1\rangle + 0.09\|\mp 5\rangle$	
$0.60\|6\rangle + 0.52\|0\rangle + 0.60\|-6\rangle$	23.6
$Tb(OH)_3$	
$0.71\|6\rangle + 0.05\|0\rangle + 0.71\|-6\rangle$	
$0.71\|6\rangle - 0.71\|-6\rangle$	0.49
$0.99\|\pm 5\rangle + 0.13\|\mp 1\rangle$	122.06
$Tb{:}Y(OH)_3$	
$0.71\|6\rangle + 0.06\|0\rangle + 0.71\|-6\rangle$	
$0.71\|6\rangle - 0.71\|-6\rangle$	0.58
$0.99\|\pm 5\rangle + 0.16\|\mp 1\rangle$	115.33

[a]Reference 65.

calculations as done for $LiHoF_4$ in Refs. 6 and 7. As suggested in Refs. 6, the accuracy of any future calculations (mean field or quantum Monte Carlo) could be improved by the use of directly measured accurate values of the transverse-field splitting of the ground-state doublet instead of the less certain values calculated from CFP.

Since our main goal in this exploratory work is to estimate the critical transverse field, B_x^c, for the family of $RE(OH)_3$ compounds and to explore the possible validity of a transverse-field Ising model description of these materials, we henceforth restrict ourselves to the $\mathcal{H}_{cf}$ in Eq. (2) with the CFP (B_n^m parameter values) given in Table IV. These calculations could be revisited, and quantum Monte Carlo simulations[6,7] performed once experimental results reporting on the effect of B_x on $Dy(OH)_3$ and $Ho(OH)_3$ become available.

C. Single-ion transverse-field spectrum

A magnetic field, B_x, applied in the direction transverse to the easy axis splits the degeneracy of the ground-state doublet in the case of $Ho(OH)_3$ and $Dy(OH)_3$ or increase the separation of the ground levels in the case of the already weakly separated singlets in $Tb(OH)_3$. By diagonalizing the single-ion Hamiltonian, $\mathcal{H}_0$, which consist of the crystal field and Zeeman terms,

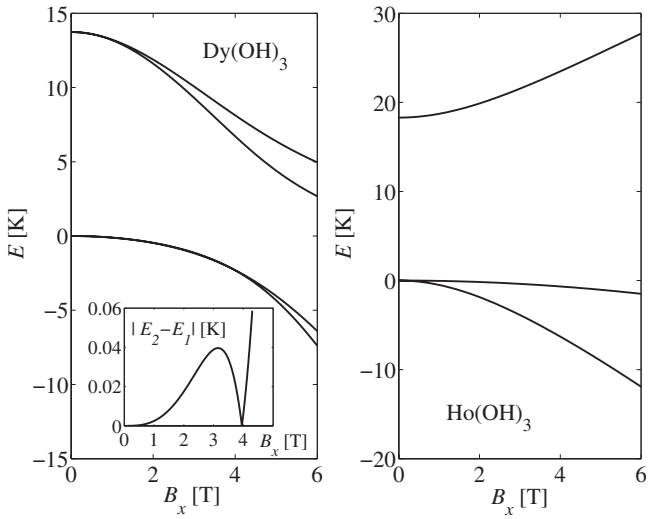

FIG. 2. Energy levels as a function of applied transverse field for $Dy(OH)_3$ and $Ho(OH)_3$. The inset shows the separation of the lowest-energy levels in $Dy(OH)_3$.

$$\mathcal{H}_0 = \mathcal{H}_{cf}(\boldsymbol{J}_i) - g\mu_B B_x J_x, \tag{4}$$

we obtain the transverse-field dependence of the single-ion energy levels plotted in Fig. 2. In the case of $Dy(OH)_3$, the two lowest-energy levels splitting is too small to be clearly visible in the main panel of Fig. 2. Hence, we show the energy separation between the two lowest levels in the inset of Fig. 2 for $Dy(OH)_3$. Furthermore, the separation vanishes at $B_x = 3.92$ T indicating that the two lowest states for this specific value of the transverse field, B_x, are degenerate.

To calculate the transverse-field dependence of the lowest-energy levels up to the critical transverse field where dipolar ferromagnetism is destroyed, we do not have to include all the crystal-field states since the B_x-induced admixing among the states decreases with increasing energy separation. In the case of $Ho(OH)_3$ we can reproduce fairly accurately the field dependence, B_x, of the energy, E, of the lowest-energy levels in Fig. 2 using only the four lowest levels. However, in order to achieve a similar level of agreement for $Dy(OH)_3$, we have to retain the ground doublet and several of the lowest excited doublets.

III. NUMERICAL SOLUTION

The collective magnetic properties of the considered rare-earth hydroxides are mainly controlled by a long-range dipolar interaction between the magnetic moments carried by the rare-earth ions. The dipolar interaction is complemented by a short-range exchange interaction. Adding the interaction terms to the single-ion Hamiltonian (4) gives a full Hamiltonian, $\mathcal{H}$, of the form

TABLE VI. Dimensionless lattice sums calculated with the values of c/a taken from Table II.

	L_{xx}	L_{yy}	L_{zz}
$Tb(OH)_3$	−11.43	−11.43	−28.01
$Dy(OH)_3$	−11.40	−11.41	−28.20
$Ho(OH)_3$	−11.38	−11.37	−28.45

$$\mathcal{H} = \sum_i \mathcal{H}_{\rm cf}(\boldsymbol{J}_i) - g\mu_{\rm B}\sum_i B_x J_{i,x} + \frac{1}{2}\sum_{ij}\sum_{\mu\nu}\mathcal{L}_{ij}^{\mu\nu} J_{i,\mu} J_{j,\nu} + \frac{1}{2}\mathcal{J}_{\rm ex}\sum_{i,{\rm nn}} \boldsymbol{J}_i \cdot \boldsymbol{J}_{\rm nn}. \quad (5)$$

$\mathcal{L}_{ij}^{\mu\nu}$ are the anisotropic dipole-dipole interaction constants of the form $\mathcal{L}_{ij}^{\mu\nu} = \frac{\mu_0 (g\mu_{\rm B})^2}{4\pi a^3} L_{ij}^{\mu\nu}$, where $\mu, \nu = x, y, z$, a is a lattice constant (see Table II), and μ_0 is the permeability of vacuum. $L_{ij}^{\mu\nu}$ are dimensionless dipolar interaction coefficients,

$$L_{ij}^{\mu\nu} = \frac{\delta^{\mu\nu}|\boldsymbol{r}_{ij}|^2 - 3(\boldsymbol{r}_{ij})^\mu (\boldsymbol{r}_{ij})^\nu}{|\boldsymbol{r}_{ij}|^5}, \quad (6)$$

where $\boldsymbol{r}_{ij} = \boldsymbol{r}_j - \boldsymbol{r}_i$, with $\boldsymbol{r}_i$ the lattice position of magnetic moment $\boldsymbol{J}_i$ expressed in units of the lattice constant a. $\mathcal{J}_{\rm ex}$ is the antiferromagnetic ($\mathcal{J}_{\rm ex} > 0$) exchange interaction constant, which can be recast as $\mathcal{J}_{\rm ex} = \frac{\mu_0 (g\mu_{\rm B})^2}{4\pi a^3} J_{\rm ex}$, where $J_{\rm ex}$ is now a dimensionless exchange constant that, when multiplied by the nearest-neighbor coordination number, $z=6$, can be used to compare the relative strength of exchange vs the magnetic dipolar lattice sum (energies) collected in Table VI. The label nn in Eq. (5) denotes the nearest-neighbor sites of site i.

The exchange interaction is expected to be of somewhat lower strength than the dipolar coupling.[55,67] We therefore neglect it in most of the calculations, but we discuss its effect on the calculated B_x vs T phase diagram at the end of this section as well as explore its influence on the occurrence of a first-order phase transition in $Dy(OH)_3$ in Sec. V B. Denoting $L_{\mu\nu} = \Sigma_j L_{ij}^{\mu\nu}$ and $\mathcal{L}_{\mu\nu} = \frac{\mu_0 (g\mu_{\rm B})^2}{4\pi a^3} L_{\mu\nu}$, we write a mean-field Hamiltonian in the form

$$\mathcal{H}_{\rm MF} = \mathcal{H}_c(\boldsymbol{J}) - g\mu_{\rm B} B_x J_x + \sum_{\mu=x,y,z} (\mathcal{L}_{\mu\mu} + z\mathcal{J}_{\rm ex}) \times \left(J_\mu \langle J_\mu \rangle - \frac{1}{2}\langle J_\mu \rangle^2 \right), \quad (7)$$

with $z=6$ the number of nearest neighbors. The last term in Eq. (7), $-\frac{1}{2}\langle J_\mu \rangle^2$, has no effect on the calculated thermal expectation values of the $\hat{x}$ and $\hat{z}$ components of the magnetization and can be dropped. The off-diagonal terms, $\mathcal{L}_{\mu\nu}$ with $\mu \neq \nu$, vanish due to the lattice symmetry. We employ the Ewald technique[68–72] to calculate the dipole-dipole interaction, $L_{ij}^{\mu\nu}$, of Eq. (6). By summing over all sites j coupled to an arbitrary site i, we obtain the coefficients $L_{\mu\nu}$ listed in Table VI. The considered Ewald sums ignore a demagnetization term,[72] and our calculations can therefore be interpreted as corresponding to a long needle-shape sample.

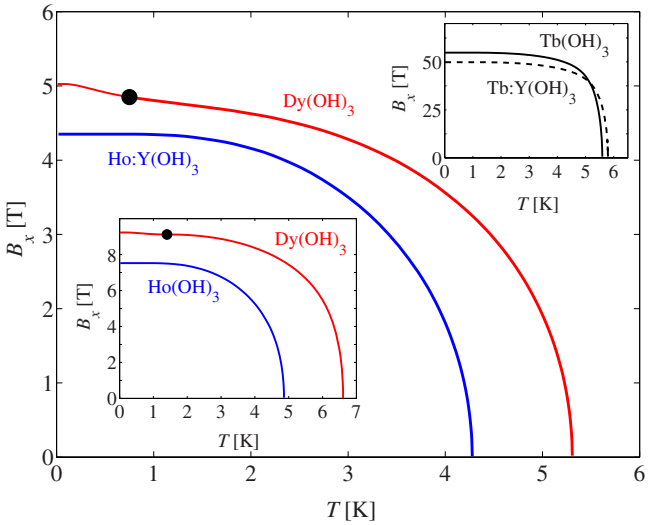

FIG. 3. (Color online) The main panel shows the phase diagrams for $Dy(OH)_3$ and Ho:Y$(OH)_3$ [crystal-field parameters of Scott *et al.*(Refs. 56 and 60)]. The dot indicates the location of the tricritical point for $Dy(OH)_3$. The transition is first order for temperatures below the temperature location of the tricritical point. The upper inset shows the phase diagram for $Tb(OH)_3$ [crystal-field parameters of Scott *et al.*(Refs. 56, 59, and 64)]. The lower inset shows the phase diagram for $Ho(OH)_3$ and $Dy(OH)_3$ calculated with the crystal-field parameters of Karmakar *et al.* (Refs. 65 and 66).

We diagonalize numerically $\mathcal{H}_{\rm MF}$ in Eq. (7) and calculate self-consistently the thermal averages of J_x and J_z operators from the expression,

$$\langle J_\mu \rangle = \frac{{\rm Tr}[J_\mu \exp(-\mathcal{H}_{\rm MF}/T)]}{{\rm Tr}[\exp(-\mathcal{H}_{\rm MF}/T)]}, \quad (8)$$

where μ stands for x and z. $\langle J_y \rangle = 0$ due to the lattice mirror symmetries and since $\boldsymbol{B}$ is applied along $\hat{x}$.

For a given B_x, we find the value of the critical temperature, $T_c(B_x)$, at which the order parameter, $\langle J_z \rangle$, vanishes. The resulting B_x vs T phase diagrams, obtained that way using *all* sets of CFP from Table IV, are shown in Fig. 3. In the main panel, we plot the phase diagrams for $Ho(OH)_3$ and $Dy(OH)_3$ using CFP of Scott *et al.*[56,59,60,64] The top inset shows the B_x vs T phase diagrams for $Tb(OH)_3$ using two available sets of CFP. These indicate that for $Tb(OH)_3$, the critical field, $B_x(T)$, reaches very quickly the upper limit of magnetic fields attainable with commercial magnets. The bottom inset shows the B_x vs T phase diagrams for $Ho(OH)_3$ and $Dy(OH)_3$ using CFP of Karmakar *et al.*[65,66] Although the diagrams differ quantitatively for the two sets of CFP, the overall qualitative trend is the same for both sets. Table VII lists the mean-field estimates of T_c and B_x^c together with the experimental values of T_c.[55,67,73]

There are two contributing factors behind the difference between the experimental and mean-field values of T_c in Table VII and, presumably, once they are experimentally determined, those for B_x^c. First, in obtaining those mean-field values from Eqs. (7) and (8), we neglected the (presumably) antiferromagnetic nearest-neighbor exchange, $\mathcal{J}_{\rm ex}$, which

TABLE VII. Experimental values of critical temperatures T_c (Refs. 55 and 67) and MFT estimates for T_c and B_x^c.

Crystal	Experimental T_c (K)	MFT T_c (K)	MFT B_x^c (T)
$Ho(OH)_3$	2.54	4.28	4.35
$Dy(OH)_3$	3.48	5.31	5.03
$Tb(OH)_3$	3.72	5.59	54.81

would contribute to a depression of both the critical ferromagnetic temperature, T_c, and B_x^c. Second, mean-field theory neglects correlations in the thermal and quantum fluctuations which would also contribute in reducing T_c and B_x. From the comparison of mean-field theory[6] and quantum Monte Carlo[6,7] for $LiHoF_4$, we would anticipate that our mean-field estimates of T_c and B_x are accurate within 20%–40%, not withstanding the uncertainty on the crystal-field parameters.

By seeking a self-consistent solution for $\langle J_z \rangle$, starting from either the fully polarized or weakly polarized state, two branches of solutions are obtained at low temperature and large B_x for $Dy(OH)_3$. This suggests a first-order PM to FM transition when using either set of CFP for this material. This result was confirmed by a more thorough investigation (see Sec. V below). The top right inset of Fig. 7 shows the behavior of the $\langle J_z \rangle$ as a function of B_x for $T=0.3$ K illustrating the transition field and the limits for the superheating and supercooling regime. The black dot in the main panel and inset of Fig. 3 shows the location of the tricritical point (TCP) (see Sec. V). Note that the B_x value at the tricritical point is ~ 4.85 T using the CFP of Scott *et al.*[56,59,60,64] (main panel of Fig. 3). Hence, the occurrence of a first-order transition here is not directly connected to the degeneracy occurring between the two lowest-energy levels at $B_x=3.92$ T using the same set of CFP [see inset of Fig. 2 for $Dy(OH)_3$]. A zoom on the low-temperature regime and the vicinity of the tricritical point for $Dy(OH)_3$ are shown in Fig. 7. The calculation details needed to obtain the phase diagram of Fig. 7 are described in Sec. V A. The existence of a first-order transition at strong B_x in $Dy(OH)_3$ depends on the details of the chosen Hamiltonian in Eq. (5). For example, as discussed in Sec. V B, a sufficiently strong nearest-neighbor antiferromagnetic exchange, $\mathcal{J}_{ex}$, eliminates the first-order transition. We also discuss in Sec. V B the role of a longitudinal field, B_z, (along the c axis) on the first-order transition. At this time, one must await experimental results to ascertain the specific low-temperature behavior that is at play for strong B_x in $Dy(OH)_3$.

We now briefly analyze the effect of a nonzero exchange interaction. The dependence of the critical temperature, T_c, and the critical transverse field, B_x^c, on the exchange constant, J_{ex}, is plotted in Fig. 4. The dot on the B_x vs J_{ex} plot for $Dy(OH)_3$ indicates the threshold value of J_{ex}, $J_{ex}^{2nd}=0.995$, above which the first-order transition ceases to exist. The dependence of the existence of the first-order transition on J_{ex} is discussed in some detail in Sec. V B. For $J_{ex}<J_{ex}^{2nd}$, the thinner lines correspond to the boundary of the supercooling and superheating regimes. In the mean-field theory presented here, J_{ex} simply adds to the interaction constant $\mathcal{L}_{\mu\mu}$ with

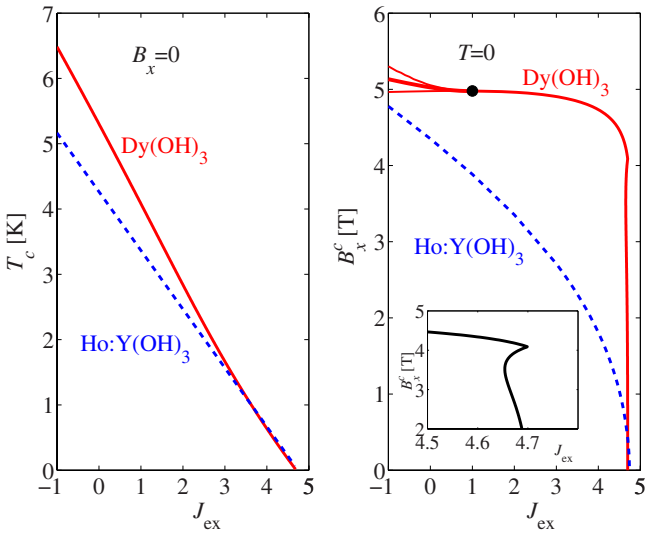

FIG. 4. (Color online) The effect of the value of the exchange constant on the phase boundary, T_c vs J_{ex} at $B_x=0$ (left) and B_x^c vs J_{ex} at $T=0$ (right). Solid and dashed lines are used for $Dy(OH)_3$ and $Ho(OH)_3$, respectively. The inset of the right graph shows a focus on the features of the high J_{ex} regime in the $Dy(OH)_3$ plot. The dot in the right panel indicates the tricritical point. The two additional lines at the left side of the tricritical point mark the limits of superheating and supercooling regimes. In the calculations, the CFP of Ref. 56 were used.

$\mu=x,y,z$ in Eq. (7) (see Table VI). Hence, beyond a threshold value of J_{ex}, the system no longer admits a long-range ordered ferromagnetic phase. In the case of $Dy(OH)_3$, B_x^c stays almost unchanged as a function of J_{ex} until it drops very sharply when $\mathcal{L}_{zz}+z\mathcal{J}_{ex}=0$ ($z=6$). In the inset of Fig. 4, we focus on the regime where B_x^c vs J_{ex} plot sharply drops. The cusp at $B_x=3.92$ T is a consequence of the degeneracy of the lowest-energy eigenstates (see Fig. 2). The reentrance from FM to PM seen in the inset of the right panel of Fig. 4 as B_x is varied for $J_{ex}\sim 4.7$ can be understood as follows. At constant $J_{ex}\sim 4.7$, with increasing B_x, the splitting of the ground doublet, which is at the origin of the quantum fluctuations, increases and at, let's say $B_x\sim 2$ T, there is a transition to quantum paramagnet. When B_x approaches the degeneracy point at ~ 3.92 T, the gap then *decreases*, as illustrated in the inset of the left panel of Fig. 2, and there is a transition back to the FM phase. Beyond the energy level crossing ($B_x>3.92$ T), the energy gap increases again and a final transition to a quantum paramagnet occurs. This phenomenology is only possible when the nearest-neighbor antiferromagnetic exchange almost cancels the dipolar interactions. It would therefore appear very unlikely that the real $Dy(OH)_3$ material would display this effect. As will be shown in Sec. IV for the $Ho(OH)_3$ system, the energy gap separating the transverse-field-splitted levels of the ground-state doublet plays the role of an effective transverse field, $\Gamma(B_x)$, acting on effective Ising spins.

IV. EFFECTIVE $S=1/2$ HAMILTONIAN

In this section we show that $Ho(OH)_3$ and $Tb(OH)_3$ can be described with good accuracy by an effective TFIM

Hamiltonian. On the other hand, although $Dy(OH)_3$ has been referred in the literature as an Ising material,[67,74] we find that it is not possible to describe the magnetic properties of this material within the framework of an effective microscopic Ising Hamiltonian that neglects the effect of the excited crystal-field states.

To be able to identify a material as a realization of an effective *microscopic* Ising model, the following conditions should apply:[75]

(i) There has to be a ground-state doublet or a close pair of singlets that are separated from the next energy level by an energy gap that is large in comparison with the critical temperature. This ensures that at the temperatures of interest only the two lowest levels are significantly populated.

(ii) To first order, there has to be no transverse susceptibility. It means that there should be no matrix elements of the (J_x, J_y) operators between the two states of the ground doublet.

(iii) Furthermore, the longitudinal (in the easy axis direction) susceptibility has to be predominantly controlled by the two lowest levels. In other words, there has to be no significant mixing of the states of the lowest doublet with the higher levels via the internal mean field along the Ising direction. In more technical terms, the van Vleck susceptibility should play a negligible role to the noninteracting (free ion) susceptibility near the critical temperature.[76]

(iv) In setting up the above conditions, one is in effect requesting that a material be describable as a TFIM from a microscopic point of view. However, one can, alternatively, ask whether the quantum critical point of a given material is in the same universality class as the relevant transverse-field Ising model. In such a case, as long as transition is second order, sufficiently close to the quantum critical point, a mapping to an effective TFIM is always in principle possible. However, it can be difficult to estimate the pertinent parameters entering the Ginzburg-Landau-Wilson theory describing the transition.

The first condition (i) above is not satisfied in the case of $Dy(OH)_3$. The energy gap of 7.8 $cm^{-1} \approx 11.2$ K is not much larger than the mean-field critical temperature $T_c \sim 5.31$ K. Hence, at temperatures close to T_c, the first excited doublet state is also significantly populated. Furthermore and most importantly in the context of a field-induced quantum phase transition, the third condition (iii) above is also not satisfied. Hence, even at low temperatures, because of the admixing of the two lowest-energy states with the higher-energy levels that is induced via the internal (mean) field from the surrounding ions, $Dy(OH)_3$ cannot be described by an effective *microscopic* Ising model that solely considers the ground doublet and ignores the excited crystal-field states. This effect and the associated role of nonzero J_z matrix elements between the ground-state and higher crystal-field levels are discussed in more detail in the Appendix. As an interesting consequence of this participation of the higher-energy levels, we predict that unlike in the TFIM of Eq. (1), a first-order phase transition may occur at high transverse field in $Dy(OH)_3$ (see Sec. V A).

For $Ho(OH)_3$ and $Tb(OH)_3$ we construct an effective Ising Hamiltonian, following the method of Refs. 6–8. We diagonalize exactly the noninteracting Hamiltonian, $\mathcal{H}_0$ of Eq. (4), for each value of the transverse field, B_x. We denote the two lowest states by $|\alpha(B_x)\rangle$ and $|\beta(B_x)\rangle$ and their energies by $E_\alpha(B_x)$ and $E_\beta(B_x)$, respectively. A transverse field introduces a natural basis choice where the states can be interpreted as $|\rightarrow\rangle$ and $|\leftarrow\rangle$ in the Ising subspace. We introduce the $|\uparrow\rangle$ and $|\downarrow\rangle$ basis, in which the J_z matrix elements are diagonal, by performing a rotation,

$$|\uparrow\rangle = \frac{1}{\sqrt{2}}[|\alpha(B_x)\rangle + \exp(i\theta)|\beta(B_x)\rangle],$$

$$|\downarrow\rangle = \frac{1}{\sqrt{2}}[|\alpha(B_x)\rangle - \exp(i\theta)|\beta(B_x)\rangle]. \tag{9}$$

In this basis, the effective single-ion Hamiltonian describing the two lowest states is of the form

$$\mathcal{H}_T = \bar{E}(B_x) - \frac{1}{2}\Delta(B_x)\sigma^x, \tag{10}$$

where $\bar{E}(B_x) = \frac{1}{2}[E_\alpha(B_x) + E_\beta(B_x)]$ and $\Delta(B_x) = E_\beta(B_x) - E_\alpha(B_x)$. Thus, the splitting of the ground-state doublet plays the role of a transverse magnetic field, $\Gamma \equiv \frac{1}{2}\Delta(B_x)$ in Eq. (1). In the case of $Tb(OH)_3$, after performing rotation (9), even at $B_x = 0$, a small transverse-field term $[\Gamma = \frac{1}{2}\Delta(0) > 0]$ is present in Hamiltonian (10). For $Dy(OH)_3$ and $Ho(OH)_3$, the splitting of the energy levels obtained via exact diagonalization was already discussed at the end of Sec. II and is shown in Fig. 2. To include the interaction terms in our Ising Hamiltonian, we expand the matrix elements of J_x, J_y, and J_z operators in terms of the σ^ν $(\nu = x, y, z)$ Pauli matrices and a unit matrix, $\sigma^0 \equiv \mathbb{1}$,

$$J_{i,\mu} = C_\mu \mathbb{1} + \sum_{\nu=x,y,z} C_{\mu\nu}(B_x)\sigma_i^\nu. \tag{11}$$

By replacing all $J_{i,\mu}$ operators in the interaction term of Hamiltonian (5) by the two-dimensional representation of Eq. (11), one obtains in general a lengthy Hamiltonian containing all possible combinations of spin-1/2 interactions.[7,8] In the present case, the resulting Hamiltonian is considerably simplified by the crystal symmetries and the consequential vanishing of off-diagonal elements of the interaction matrix $\mathcal{L}_{\mu\nu}$. This would not be the case for diluted $LiHo_xY_{1-x}F_4$ (see Ref. 8). After performing the transformation in Eq. (11), we have $J_i^z = C_{zz}\sigma_i^z$, $J_i^y = C_{yy}\sigma_i^y$, and $J_i^x = C_{xx}\sigma_i^x + C_x\mathbb{1}$. Hence, we can rewrite the mean-field Hamiltonian (7) in the form

$$\mathcal{H}_{\mathrm{MF}} = (\mathcal{L}_{zz} + z\mathcal{J}_{\mathrm{ex}})C_{zz}^2 m_z \sigma^z + \left(\mathcal{L}_{xx}C_x C_{xx} - \frac{1}{2}\Delta(B_x)\right)\sigma^x + (\mathcal{L}_{xx} + z\mathcal{J}_{\mathrm{ex}})C_{xx}^2 m_x \sigma^x + (\mathcal{L}_{yy} + z\mathcal{J}_{\mathrm{ex}})C_{yy}^2 m_y \sigma^y, \tag{12}$$

where $m_\nu \equiv \langle\sigma^\nu\rangle$ and $\langle\cdots\rangle$ denotes a Boltzmann thermal average. Here we have dropped terms proportional to m_x^2 and m_z^2.

The C_{zz}, C_{xx}, and C_x coefficients for $Ho(OH)_3$ are plotted in Fig. 5. The inset shows a comparison of the terms in $\mathcal{H}_{\mathrm{MF}}$. In $Ho(OH)_3$, the coefficient $\mathcal{L}_{xx}C_{xx}^2$ (the fourth term of $\mathcal{H}_{\mathrm{mf}}$ for $\mathcal{J}_{\mathrm{ex}} = 0$) does not exceed 1.5% of the effective transverse

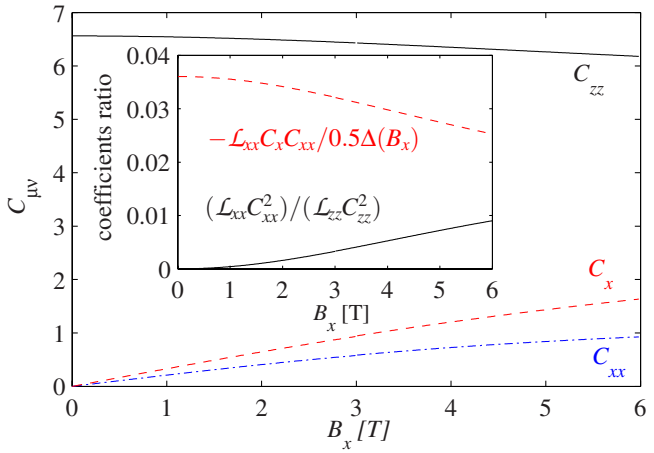

FIG. 5. (Color online) The coefficients in the projection of $\boldsymbol{J}$ operators onto the two-dimensional Ising subspace for $Ho(OH)_3$. The inset shows the ratios of the coefficients present in Eq. (12).

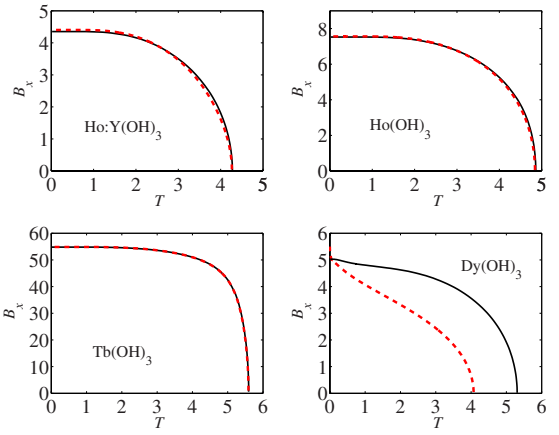

FIG. 6. (Color online) Comparison of the phase diagrams obtained with diagonalization of the full manifold (black solid lines) and with effective spin-1/2 Hamiltonian (red dashed lines). Calculation for $Ho(OH)_3$ were performed using the CFP of Karmakar *et al.* (Refs. 65 and 66).

field, $\Gamma=\mathcal{L}_{xx}C_xC_{xx}-\frac{1}{2}\Delta(B_x)$. In $Tb(OH)_3$, this ratio is even smaller, and we thus neglect it, further motivated by the fact that doing so decouples m_z from m_x, making the problem simpler. The term $\mathcal{L}_{yy}C_{yy}^2m_y\sigma^y$ in Eq. (12) can be omitted since, due to symmetry, $m_y\equiv\langle\sigma^y\rangle=0$. The interaction correction, $\mathcal{L}_{xx}C_xC_{xx}$, to the effective transverse field, Γ, is of order of 3% of Γ, and we retain it in our calculations. Thus, we finally write,

$$\mathcal{H}_{\mathrm{MF}}=P\sigma^z+\Gamma\sigma^x, \tag{13}$$

where $P=(\mathcal{L}_{zz}+z\mathcal{J}_{\mathrm{ex}})C_{zz}^2m_z$ and $\Gamma=\mathcal{L}_{xx}C_xC_{xx}-\frac{1}{2}\Delta(B_x)$.

Diagonalizing Hamiltonian (13) allows us to evaluate m_z and $m_x\equiv\langle\sigma^x\rangle$, giving well-known formulas,[4]

$$m_x=\frac{\Gamma}{\sqrt{P^2+\Gamma^2}}\tanh(\sqrt{P^2+\Gamma^2}/T),$$

$$m_z=\frac{P}{\sqrt{P^2+\Gamma^2}}\tanh(\sqrt{P^2+\Gamma^2}/T), \tag{14}$$

and the phase boundary,

$$T_c(B_x)=\frac{\Gamma(B_x)}{\operatorname{arctanh}\left(\dfrac{\Gamma(B_x)}{(\mathcal{L}_{zz}+z\mathcal{J}_{\mathrm{ex}})C_{zz}^2}\right)}. \tag{15}$$

In Fig. 6, we show that Eq. (15) yields a phase diagram that only insignificantly differs from the one obtained from the full diagonalization of $\mathcal{H}_{\mathrm{MF}}$ in Eq. (7), shown in Fig. 3, in the case of $Ho(OH)_3$. In the case of $Tb(OH)_3$, the discrepancy is even smaller because the energy gap to the third crystal-field state, 118 $\mathrm{cm}^{-1}\simeq 170$ K, is very large compared to $T_c^{\mathrm{MF}}=5.59$ K.

As alluded above, in the case of $Dy(OH)_3$, a description in terms of an effective Ising Hamiltonian method does not work because of the admixing between states of the two lowest doublets induced by the local mean-field that is proportional to $\langle J_z\rangle$ (see Appendix). The dashed line in the bottom right panel of Fig. 6 shows the incorrect phase diagram obtained for $Dy(OH)_3$ using an effective spin-1/2 Hamiltonian constructed only from the ground doublet. It turns out that a form of the method of Sec. IV can still be used. However, instead of keeping only two levels in the interaction Hamiltonian, one needs to retain at least four states. In analogy with the procedure in Sec. IV, we diagonalize the single-ion Hamiltonian $\mathcal{H}_0$ of Eq. (4), which consists of the crystal-field Hamiltonian and the transverse-field term. Next, we write an effective interaction Hamiltonian using the four (or six) lowest eigenstates of $\mathcal{H}_0$. The resulting effective Hamiltonian is then used in the self-consistent Eq. (8). For example, for $B_x=4.8$ T, proceeding by keeping only the four lowest eigenstates of $\mathcal{H}_0$ to construct the effective Hamiltonian, one finds a critical temperature that is only about 3% off compared to a calculation that keeps all 16 eigenstates of $\mathcal{H}_0$. This difference drops below 1% when keeping the six lowest eigenstates of $\mathcal{H}_0$.

Having explored the quantitative validity of the spin-1/2 TFIM description of $Ho(OH)_3$ and $Tb(OH)_3$ in nonzero B_x, we now turn to the problem of the first-order PM to FM transition at large B_x and low temperature in $Dy(OH)_3$ exposed in the numerical solution of the self-consistent equations comprised by Eqs. (7) and (8) (with $\mu=x,z$).

V. FIRST-ORDER TRANSITION

The first-order transition in $Dy(OH)_3$ takes its origin in the sizeable admixing among the four lowest levels that is induced by the local mean-field that is proportional to $\langle J_z\rangle$. Under the right temperature and field conditions, two free-energy equivalent configurations can exist: an ordered state with some not infinitesimally small magnetization, $\langle J_z\rangle>0$, and a state with zero magnetic moment, $\langle J_z\rangle=0$. To simplify the argument, we consider how this occurs at $T=0$. First, let us look at the situation when the longitudinal internal mean field induces an admixing of the ground state with the first excited state only (as in the TFIM). In such a case, there is only a quadratic dependence of the ground-state energy on

the longitudinal mean field, B_z^{MF}, and consequently, only one energy minimum is possible. Now, if there is an admixing of the ground state and at least three higher levels, the dependency of the ground-state energy on B_z^{MF} is of fourth order and two energy minima are, in principle, possible. Thus, at a certain value of external parameters the system can acquire two energetically equivalent states, one with zero and the other with a nonzero magnetization. When passing through this point, either by varying the transverse field, B_x, or the temperature, a first-order phase transition characterized by a magnetization discontinuity occurs. To make this discussion more formal, we proceed with a construction of the Ginzburg-Landau theory for $Dy(OH)_3$ for arbitrary B_x, in the regime of B_x and T values where the paramagnetic to ferromagnetic transition is second order. This allows us to determine the tricritical transverse-field value above which the transition becomes first order.

A. Ginzburg-Landau theory

To locate the tricritical point for $Dy(OH)_3$, we perform a Landau expansion of the mean-field free energy, $\mathcal{F}_{\mathrm{MF}}(\langle J_x\rangle,\langle J_z\rangle)$. Next, we minimize $\mathcal{F}_{\mathrm{MF}}$ with respect to $\langle J_x\rangle$ leaving $\langle J_z\rangle$ as the only free parameter. The mean-field free energy can be written in the form

$$\mathcal{F}_{\mathrm{MF}}(\langle J_x\rangle,\langle J_z\rangle) = -T\log Z(\langle J_x\rangle,\langle J_z\rangle) - \frac{1}{2}(\mathcal{L}_{xx}\langle J_x\rangle^2 + \mathcal{L}_{zz}\langle J_z\rangle^2), \tag{16}$$

where $Z(\langle J_x\rangle,\langle J_z\rangle)$ is the partition function.

Just below the transition, in the part of the phase diagram where the transition is second order, $\langle J_z\rangle$ is a small parameter (i.e., has a small dimensionless numerical value). We therefore make an expansion for $\langle J_x\rangle$ as a function of $\langle J_z\rangle$, which we write in the form

$$\langle J_x\rangle = \langle J_x\rangle_0 + \delta(\langle J_z\rangle). \tag{17}$$

$\langle J_x\rangle_0$ is the value of $\langle J_x\rangle$ that extremizes $\mathcal{F}_{\mathrm{MF}}$ when $\langle J_z\rangle=0$. $\delta(\langle J_z\rangle)$ is a perturbatively small function of $\langle J_z\rangle$, which we henceforth simply denote as δ and which is our small parameter series expansion for $\langle J_x\rangle$. Substituting expression (17) into $\mathcal{H}_{\mathrm{MF}}$ of Eq. (7) and setting $\mathcal{J}_{\mathrm{ex}}=0$ for the time being, we have

$$\mathcal{H} = \mathcal{H}_{\mathrm{cf}}(\boldsymbol{J}_i) - g\mu_{\mathrm{B}}B_xJ_x + \mathcal{L}_{xx}J_x(\langle J_x\rangle_0 + \delta) + \mathcal{L}_{zz}J_z\langle J_z\rangle, \tag{18}$$

or

$$\mathcal{H} = \mathcal{H}_0(B_x,\langle J_x\rangle_0) + \mathcal{L}_{xx}J_x\delta + \mathcal{L}_{zz}J_z\langle J_z\rangle, \tag{19}$$

where for brevity, as in Eq. (7), the constant term proportional to $\langle J_x\rangle^2$ has been dropped because, again, it does not affect the expectation values needed for the calculation.

The power-series expansion of the partition function, and then of the free energy, Eq. (16), can be calculated from the eigenvalues of Hamiltonian (19). Instead of applying standard quantum-mechanical perturbation methods to Eq. (19), we obtain the expansion of energy levels as a perturbative, "seminumerical," solution to the characteristic polynomial equation,

$$\det[\mathcal{H}_0 + \mathcal{L}_{xx}J_x\delta + \mathcal{L}_{zz}J_z\langle J_z\rangle - E_n] = 0. \tag{20}$$

We can easily implement this procedure by using a computer algebra method (e.g., MAPLE™ or MATHEMATICA™). To proceed, we substitute a formal power-series expansion of the solution,

$$E_n = E_n^{(0,0)} + E_n^{(0,1)}\delta + E_n^{(2,0)}\langle J_z\rangle^2 + E_n^{(2,1)}\langle J_z\rangle^2\delta + \cdots, \tag{21}$$

into Eq. (20), containing all the terms of the form $E_n^{(\alpha,\beta)}\langle J_z\rangle^\alpha\delta^\beta$, where $\alpha+2\beta\leq 6$, as will be justified below Eq. (24). To impose consistency of the resulting equation obtained from Eqs. (20) and (21), up to sixth order of the expansion in $\langle J_z\rangle$, we need to equate to zero all the coefficients with the required order of $\langle J_z\rangle$ and δ, i.e., $\alpha+2\beta\leq 6$. This gives a system of equations that can be numerically solved for the coefficients $E_n^{(k,l)}$, where $k,l>0$. By $E_n^{(0,0)}$ we denote the eigenvalues of the Hamiltonian $\mathcal{H}_0(B_x,\langle J_x\rangle_0)$.

We use the perturbed energies, E_n, of Eq. (21) to calculate the partition function,

$$Z(\delta,\langle J_z\rangle) = \sum_n e^{-E_n/T}, \tag{22}$$

and substitute it in Eq. (16). We Taylor expand the resulting expression to obtain the numerical values of the expansion coefficients in the form,

$$\mathcal{F}_{\mathrm{MF}} = A^{(0,0)} + A^{(2,0)}\langle J_z\rangle^2 + A^{(0,1)}\delta + A^{(2,1)}\langle J_z\rangle^2\delta + \cdots. \tag{23}$$

The free energy $\mathcal{F}_{\mathrm{MF}}$ is a symmetric function of $\langle J_z\rangle$, so expansion (23) contains only even powers of $\langle J_z\rangle$. We minimize $\mathcal{F}_{\mathrm{MF}}$ in Eq. (23) with respect to δ. To achieve this, we have to solve a high-order polynomial equation $d\mathcal{F}_{\mathrm{MF}}/d\delta=0$. Again, we do it by substituting to the equation a formal power-series solution,

$$\delta(\langle J_z\rangle) = D_2\langle J_z\rangle^2 + D_4\langle J_z\rangle^4 + \cdots, \tag{24}$$

and then solve it for the values of the expansion parameters D_n. Due to symmetry, only even powers of $\langle J_z\rangle$ are present, and from the definition of δ, the constant $\langle J_z\rangle$-independent term is equal to zero. From the form of the expansion in Eq. (24), we see that to finally obtain the free-energy expansion in powers of $\langle J_z\rangle$, up to nth order, we need to consider only the terms $\langle J_z\rangle^\alpha\delta^\beta$, where $\alpha+2\beta\leq n$. Finally, by substituting δ from Eq. (24) into Eq. (23), we obtain the power-series expansion of the free energy in the form,

$$\mathcal{F}_{\mathrm{MF}} = C_0 + C_2\langle J_z\rangle^2 + C_4\langle J_z\rangle^4 + C_6\langle J_z\rangle^6. \tag{25}$$

In the second-order transition region, the condition $C_2=0$ with $C_4>0$ parametrizes the phase boundary. The equation $C_2=C_4=0$ gives the condition for the location of the tricritical point. In the regime where $C_4<0$, the condition $C_2=0$ gives the supercooling limit. The first-order phase transition boundary is located where the free energy has the same value at both local minima. Increasing the value of the

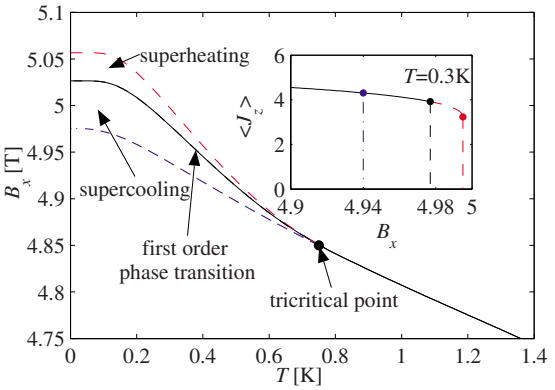

FIG. 7. (Color online) Tricritical behavior of $Dy(OH)_3$. The continuous line marks the phase boundary. The dot indicates the location of the tricritical point. The upper and lower lines (dashed lines) are the limits of the superheating and supercooling regimes, respectively. As an example, the inset shows the order parameter, $\langle J_z \rangle$, vs B_x at the temperature T=0.3 K. For this temperature, the phase transition occurs at $B_x \approx 4.98$ T. The upper dashed extension of the solid line corresponds to the superheating limit. The dash-dotted line to the left of the tricritical point shows the transition at the supercooling limit.

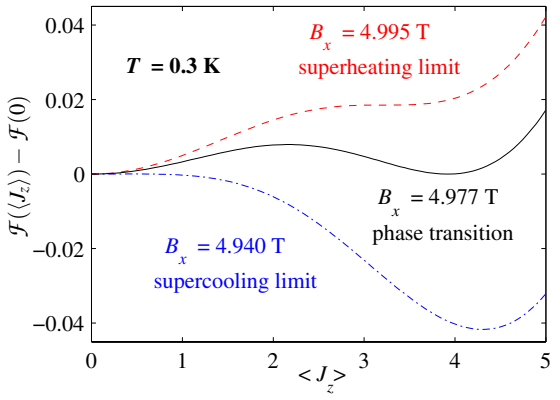

FIG. 8. (Color online) Free energy vs average magnetic moment, $\langle J_z \rangle$, at the temperature of 0.3 K. The free energy at the first-order phase transition is plotted with continuous line. The upper (dashed) line shows the free energy at the boundary of the superheating limit. The lower (dot-dashed) line shows the free energy when the system passes through the supercooling limit. All the plots show the free energy displaced by a constant chosen such that their shape can be compared.

control parameters, T and B_x, above the critical value until the second (nontrivial) local minimum of $\mathcal{F}_{\rm MF}$ vanishes, gives the superheating limit.

The location of the tricritical point is $T_c^{\rm TCP} \approx 0.75$ K and $B_x^{\rm TCP} \approx 4.85$ T. We show in Fig. 7 the first-order and the second-order transition phase boundaries; the tricritical point is marked with a dot. In the first-order transition regime, the superheating and supercooling limits are also plotted. $\langle J_z \rangle$ ceases to be a small parameter for values of T and B_x "away" from the tricritical point. Thus, the two upper curves in the phase diagram of Fig. 7 are determined from a numerical search for both local minima of the exact mean-field free energy in Eq. (16) without relying on a small $\langle J_z \rangle$ and $\delta(\langle J_z \rangle)$ expansions. The supercooling limit is calculated from the series expansion (25) and determined by the condition C_2=0.

In the inset of Fig. 7, we show the average magnetic moment, $\langle J_z \rangle$, as a function of the transverse field at the temperature of 0.3 K. The solid dots and the dashed lines mark the supercooling limit, first-order phase boundary, and the superheating limit in order of increasing B_x. The free energy at these three characteristic values of the magnetic field, B_x, at temperature of 0.3 K is shown in Fig. 8.

In Fig. 8, we plot the free energy as a function of $\langle J_z \rangle$, where $\langle J_x \rangle$ is minimizing $\mathcal{F}_{\rm MF}$ as a function of $\langle J_z \rangle$ at T=0.3 K. Free energy at the phase transition ($B_x \approx 4.977$ T) is plotted with a continuous line. The dashed and dot-dashed plots show free energy at the superheating and supercooling limits at $B_x \approx 4.995$ and 4.940 T, respectively. The free energy clearly shows the characteristic structure (e.g., barrier) of a system with a first-order transition. It would be interesting to investigate whether the real $Dy(OH)_3$ material exhibits such a B_x-induced first-order PM to FM transition at strong B_x. In the event that the transition is second order down to T=0 and $B_x = B_x^c$, $Dy(OH)_3$ would offer itself as another material to investigate transverse-field-induced quantum criticality (see fourth item of the list at the beginning of Sec. IV). However, a quantitative microscopic description at strong B_x would nevertheless require that the contribution of the lowest pairs of excited crystal-field states be taken into account.

One may be tempted to relate the existence of a first-order transition in $Dy(OH)_3$, on the basis of Eq. (23) with two expansion parameters $\langle J_z \rangle$ and δ, to the familiar problem where a free-energy function, $\mathcal{F}(m, \epsilon)$, of two order parameters m and ϵ,

$$\mathcal{F}(m,\epsilon) = \frac{a}{2}m^2 + \frac{|b|}{4}m^4 + \frac{|c|}{6}m^6 + \frac{K}{2}\epsilon^2 - g\epsilon m^2,$$

displays a first-order transition when $g^2/K > b/2$. However, we have found that this analogy is not useful, and the mechanism for the first-order transition is not trivially due to the presence of two expansion parameters, $\langle J_z \rangle$ and δ, in expansion (23). It is rather the complex specific details of the crystal-field Hamiltonian for $Dy(OH)_3$ that are responsible for the first-order transition. For example, at a qualitative level, a first-order transition still occurs even if the small $\delta(\langle J_z \rangle)$ parameter in Eq. (17) is taken to be zero at the outset for all values of $\langle J_z \rangle$.

B. Effect of longitudinal magnetic field and exchange interaction on the existence of first-order transition in $Dy(OH)_3$

Having found that the PM to FM transition may be first order in $Dy(OH)_3$ at large B_x (low T), it is of interest to investigate briefly two effects of physical relevance on the predicted first-order transition. First, since the transition is first order from $0 \le T \le T^{\rm TCP}$, one may ask what is the critical *longitudinal* field, B_z, required to push the tricritical point from finite temperature down to zero temperature. Focusing on the CFP of Scott *et al.*,[56,59,60,64] we find that a sufficiently

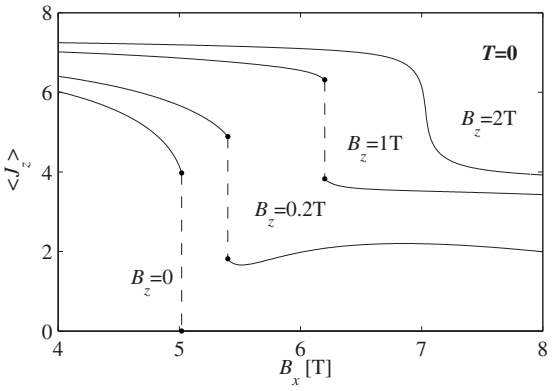

FIG. 9. Average magnetic moment, $\langle J_z \rangle$, vs transverse magnetic field, B_x, at $T=0$ and $J_{ex}=0$ for different values of longitudinal magnetic field, B_z.

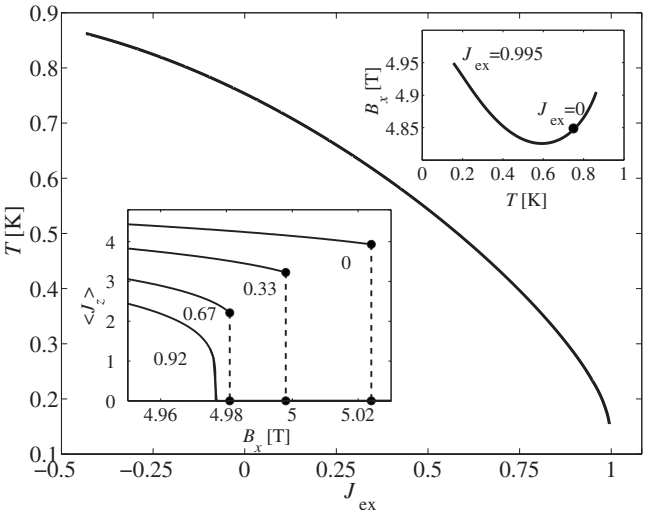

FIG. 10. Temperature corresponding to the TCP, T_c^{TCP}, as a function of nearest-neighbor exchange constant, J_{ex}. The upper inset shows the parametric position of the TCP in the phase diagram plane for the same range of exchange constant as in the main plot. For an exchange $J_{ex} > J_{ex}^{2nd}$ with $J_{ex}^{2nd}=0.995$, the tricritical point at $T>0$ ceases to exist. The lower inset shows average magnetic moment $\langle J_z \rangle$ vs transverse field B_x at temperature $T=0$ for the shown values of exchange constant J_{ex}.

strong magnetic field, B_z, applied along the longitudinal z direction destroys the first-order transition giving rise to an end critical point. We plot in Fig. 9 the magnetization, $\langle J_z \rangle$, as a function of B_x for different values of B_z at $T=0$. We see that a critical value of B_z is reached between 1 and 2 T, where the first-order transition disappears giving rise to an end critical point at $T=0$. Hence, assuming that the low-temperature B_x-driven PM to FM transition is indeed first order in $Dy(OH)_3$, the results of Fig. 9 indicate that the critical longitudinal field for a quantum critical end point should be easily accessible using a so-called vector magnet (i.e., with tunable horizontal, B_x, and vertical, B_z, magnetic fields).[77]

It was discussed in Sec. III (Fig. 4) that the (yet undetermined) nearest-neighbor exchange interaction, $\mathcal{J}_{ex}$ in Eq. (5), affects the zero B_x critical temperature, T_c, and the zero-temperature critical transverse field, B_x^c. It is also of interest to explore what is the role of $\mathcal{J}_{ex}=\frac{\mu_0(g\mu_B)^2}{4\pi}J_{ex}$ on the location (temperature and transverse field) of the tricritical point in $Dy(OH)_3$.

We plot in Fig. 10 the temperature corresponding to the TCP as a function of antiferromagnetic exchange, and in the upper inset, the location of the TCP on the phase diagram is presented. The location of the TCP was calculated using the semianalytical expansion described in Sec. V A. We found that the system ceases to exhibit a first-order transition at nonzero temperature when the value of nearest-neighbor exchange constant, J_{ex}, exceeds $J_{ex}^{2nd}=0.995$. At $B_x=0$, the critical temperature calculated with the value of exchange constant $J_{ex}=0.995$ is 4.09 K. In the lower inset of Fig. 10 we plot the average magnetic moment, $\langle J_z \rangle$, as a function of B_x at zero temperature for different values of J_{ex}. The top inset shows a parametric plot of the position of the TCP in the (T, B_x) plane as J_{ex} is varied.

VI. CONCLUSION

We have presented a simple mean-field theory aimed at motivating an experimental study of transverse-field-induced phase transitions in the insulating rare-earth Ising $RE(OH)_3$ (RE=Dy,Ho) uniaxial dipolar ferromagnetic materials.

In setting out to perform the above calculations, we were mostly motivated in identifying a class of materials as analogous as possible to $LiHo_xY_{1-x}F_4$ where interesting phenomena both in zero and nonzero applied transverse field, B_x, have been observed. In particular, we were interested in finding compounds where a systematic comparison between a non-Kramers (e.g., Ho^{3+}) and a Kramers (e.g., Dy^{3+}) variants could be investigated. From our study, we are led to suggest that an experimental study of the $Dy_xY_{1-x}(OH)_3$ and $Ho_xY_{1-x}(OH)_3$ materials could bring new pieces of information on the physics that may be at play in $LiHo_xY_{1-x}F_4$ and to ascertain if that physics is unique to $LiHo_xY_{1-x}F_4$ or if it also arises in other diluted dipolar Ising ferromagnets.

Depending on the details of the Hamiltonian characterizing $Dy(OH)_3$, it may be that a first-order transition occurs at low temperature (large B_x) due to the admixing between the ground doublet and the low-lying crystal-field states that is induced by the spin-spin interactions. Upon substitution of Dy^{3+} by Y^{3+}, the first order paramagnetic to ferromagnetic transition would likely disappear and become second order before a dipolar spin glass phase may be reached at sufficiently high Y^{3+} concentration. For the same reason, we find that $Dy(OH)_3$ is not well described by an effective microscopic transverse-field Ising model (TFIM). On the other hand, $Ho(OH)_3$ appears to be very well characterized by a TFIM and, therefore, constitutes a highly analogous variant of $LiHoF_4$. $Tb(OH)_3$ is also very well described by a TFIM. Unfortunately, in that case, the critical B_x, B_x^c, appears prohibitively large to be accessed via in-house commercial magnets.

We hope that our work will stimulate future systematic experimental investigations of these materials and, possibly, help shed some light on the rather interesting problems that

pertain to the fundamental nature of classical and quantum critical phenomena in disordered dipolar systems and which have been raised by nearly 20 years of study of $LiHo_xY_{1-x}F_4$.

ACKNOWLEDGMENTS

We thank P. Chakraborty, R. Cone, L. Corruccini, J.-Y. Fortin, S. Girvin, R. Higashinaka, R. Hill, Y. Maeno, B. Malkin, H. Molavian, V. Oganesyan, T. Rosenbaum, D. Silevitch, A. Tabei, K.-M. Tam, W. Wolf, and T. Yavors'kii for useful discussions. This work was supported by the NSERC, the Canada Research Chair Program (M.G.), the Canadian Institute for Advanced Research, the Canada Foundation for Innovation, and the Ontario Innovation Trust. M.G. thanks the University of Canterbury (UC) for funding and the hospitality of the Department of Physics and Astronomy at UC where part of this work was done.

APPENDIX: PERTURBATIVE CALCULATION OF THE PHASE DIAGRAM IN $Dy(OH)_3$

To investigate the role of the J_z matrix elements between the two lowest states and the first excited levels on the magnetic behavior of $Dy(OH)_3$, we calculate the critical temperature for a second-order transition using second-order perturbation theory. This method is exact in the second-order phase transition regime, where B_x is less than the tricritical field value, B_x^{TCP} ($B_x^{\mathrm{TCP}} \approx 4.85$ T when using the CFP of Scott *et al.* from Refs. 56 and 60).

For a given value of the transverse field, B_x, and the corresponding value of average magnetization in the transverse direction, $\langle J_x \rangle$, we consider $\mathcal{L}_{zz} J_z \langle J_z \rangle$ term as a perturbation to the reference mean-field Hamiltonian,

$$\mathcal{H}_0 = \mathcal{H}_{\mathrm{cf}}(\boldsymbol{J}_i) - g\mu_{\mathrm{B}} B_x J_x + \mathcal{L}_{xx} J_x \langle J_x \rangle, \tag{A1}$$

describing the PM phase at a temperature $T > T_c(B_x)$ as in Eq. (7). Here too, we have dropped the constant terms. The eigenvalues, E_p, and eigenstates, $|p\rangle$, of the perturbed Hamiltonian,

$$\mathcal{H} = \mathcal{H}_0 + \mathcal{L}_{zz} J_z \langle J_z \rangle, \tag{A2}$$

are written in terms of eigenvalues, $E_p^{(0)}$, and eigenstates, $|p^{(0)}\rangle$, of the unperturbed Hamiltonian, $\mathcal{H}_0$, of Eq. (A1),

$$E_p = E_p^{(0)} + \langle J_z \rangle E_p^{(1)} + \langle J_z \rangle^2 E_p^{(2)}, \tag{A3}$$

$$|p\rangle = |p^{(0)}\rangle + \langle J_z \rangle \sum_{k \neq p} c_{p,k}^{(1)} |k^{(0)}\rangle. \tag{A4}$$

The coefficients of the perturbative expansion are given by

$$E_p^{(1)} = \mathcal{L}_{zz} J_{pp}^z, \tag{A5}$$

$$E_p^{(2)} = \sum_{k \neq p} \frac{\mathcal{L}_{zz}^2 |J_{kp}^z|^2}{E_p^{(0)} - E_k^{(0)}}, \tag{A6}$$

and

$$c_{pk}^{(1)} = \frac{\mathcal{L}_{zz} J_{kp}^z}{E_p^{(0)} - E_k^{(0)}}, \tag{A7}$$

where $J_{kp}^z = \langle k^{(0)} | J_z | p^{(0)} \rangle$ are the matrix elements of the J_z operator in the basis of eigenvectors of the unperturbed Hamiltonian, $\mathcal{H}_0$. The applied magnetic field, B_x, lifts the degeneracy of the Kramers doublets; thus we can use the nondegenerate perturbation method. The diagonal elements of the J_z operator vanish; hence, the first-order correction to energy vanishes, $E_p^{(1)} = J_{pp}^z = 0$.

We calculate the thermal average of the J_z operator,

$$\langle J_z \rangle = \frac{1}{Z} \sum_p \langle p | J_z | p \rangle e^{-E_p/T}, \tag{A8}$$

using the perturbed eigenstates, $|p\rangle$, and eigenvalues, E_p, where $Z = \sum_p e^{-E_p/T}$. Keeping only terms up to third order in $\langle J_z \rangle$ in the expansion of Eq. (A8), we find

$$\frac{1}{Z} e^{-E_p/T} = n_p^{(0)} (1 + K_p \langle J_z \rangle^2) \tag{A9}$$

and

$$\langle p | J_z | p \rangle = 2 \mathcal{L}_{zz} \langle J_z \rangle \sum_{k \neq p} \frac{|J_{pk}^z|^2}{E_p^{(0)} - E_k^{(0)}}, \tag{A10}$$

where, for convenience, we write $n_p^{(0)} = e^{-E_p^{(0)}/T} / Z^{(0)}$, $Z^{(0)} = \sum_p e^{-E_p^{(0)}/T}$, and $K_p = \frac{1}{T} (\sum_k n_k^{(0)} E_k^{(2)} - E_p^{(2)})$. Thus, we can write

$$\langle J_z \rangle = 2 \langle J_z \rangle \sum_p n_p^{(0)} (1 + K_p \langle J_z \rangle^2) \sum_{k \neq p} \frac{\mathcal{L}_{zz} |J_{pk}^z|^2}{E_p^{(0)} - E_k^{(0)}}, \tag{A11}$$

and finally, we get

$$\langle J_z \rangle^2 = \frac{1 - 2 \sum_{p,k \neq p} n_p^{(0)} \dfrac{\mathcal{L}_{zz} |J_{pk}^z|^2}{E_p^{(0)} - E_k^{(0)}}}{2 \sum_{p,k \neq p} n_p^{(0)} K_p \dfrac{\mathcal{L}_{zz} |J_{pk}^z|^2}{E_p^{(0)} - E_k^{(0)}}}. \tag{A12}$$

Putting $\langle J_z \rangle = 0$ into Eq. (A12), we obtain the condition for the critical temperature, T_c, for the regime where the PM to FM transition is second order,

$$2 \sum_{p,k \neq p} \frac{\mathcal{L}_{zz} |J_{pk}^z|^2}{E_p^{(0)} - E_k^{(0)}} e^{-E_p^{(0)}/T_c} = 1. \tag{A13}$$

In solving Eq. (A13) for T_c, we have to self-consistently update the value of $\langle J_x \rangle$ in order to diagonalize $\mathcal{H}_0$ in Eq. (A1) and to find $E_p^{(0)}$. Solving Eq. (A13) with only the four lowest-energy eigenstates [after diagonalizing the full transverse-field Hamiltonian of Eq. (4)] yields a phase diagram that is in good agreement for $B_x < B_x^{\mathrm{TCP}}$ with the phase boundary obtained with all crystal-field eigenstates [or equivalently from Eq. (8)].

By estimating the values of the elements of the sum in Eq. (A13), one finds that the matrix elements of the J_z operator, mixing the two lowest states with the excited states, may bring a substantial correction to the value of the critical temperature obtained when only the two lowest eigenstates are

considered. In the low-temperature regime, one could omit the matrix elements between the states of the excited doublet, but we have to keep the matrix elements between the states of the ground doublet and first excited doublet. The contribution from the further exited states is quite small because of the increasing value of the energy gap present in the denominator of Eq. (A13).

At $T=0$, the equation for the critical transverse field, B_x^c, is

$$2\sum_{k\neq 1}\frac{\mathcal{L}_{zz}|J_{1k}^z(B_x^c)|^2}{E_1^{(0)}(B_x^c)-E_k^{(0)}(B_x^c)}=1. \tag{A14}$$

Again, we see that the matrix elements of J^z operator, admixing the ground state with the excited levels, have to be considered. Note that since Eq. (A14) pertains to the case of zero temperature, this equation is only valid in a regime where the transition is second order (i.e., when $J_{ex}>J_{ex}^{2nd}$).

[1] S. L. Sondhi, S. M. Girvin, J. P. Carini, and D. Shahar, Rev. Mod. Phys. **69**, 315 (1997).
[2] S. Sachdev, *Quantum Phase Transitions* (Cambridge University Press, Cambridge, 1999).
[3] R. J. Elliott, P. Pfeuty, and C. Wood, Phys. Rev. Lett. **25**, 443 (1970).
[4] B. K. Chakrabarti, A. Dutta, and P. Sen, *Quantum Ising Phases and Transitions in Transverse Ising Models* (Spinger-Verlag, Heidelberg, 1996).
[5] P. G. de Gennes, Solid State Commun. **1**, 132 (1963).
[6] P. B. Chakraborty, P. Henelius, H. Kjonsberg, A. W. Sandvik, and S. M. Girvin, Phys. Rev. B **70**, 144411 (2004).
[7] S. M. A. Tabei, M. J. P. Gingras, Y.-J. Kao, and T. Yavors'kii, Phys. Rev. B **78**, 184408 (2008).
[8] S. M. A. Tabei, F. Vernay, and M. J. P. Gingras, Phys. Rev. B **77**, 014432 (2008).
[9] K. Binder and A. P. Young, Rev. Mod. Phys. **58**, 801 (1986).
[10] J. A. Mydosh, *Spin Glasses: An Experimental Introduction* (Taylor & Francis, London, 1993).
[11] H. Rieger and A. P. Young, Phys. Rev. Lett. **72**, 4141 (1994).
[12] H. Rieger and A. P. Young, Phys. Rev. B **54**, 3328 (1996).
[13] M. Guo, R. N. Bhatt, and D. A. Huse, Phys. Rev. B **54**, 3336 (1996).
[14] R. B. Griffiths, Phys. Rev. Lett. **23**, 17 (1969).
[15] B. M. McCoy, Phys. Rev. Lett. **23**, 383 (1969).
[16] D. H. Reich, B. Ellman, J. Yang, T. F. Rosenbaum, G. Aeppli, and D. P. Belanger, Phys. Rev. B **42**, 4631 (1990).
[17] W. Wu, B. Ellman, T. F. Rosenbaum, G. Aeppli, and D. H. Reich, Phys. Rev. Lett. **67**, 2076 (1991).
[18] W. Wu, D. Bitko, T. F. Rosenbaum, and G. Aeppli, Phys. Rev. Lett. **71**, 1919 (1993).
[19] W. Wu, Ph.D. thesis, University of Chicago, 1992.
[20] D. Bitko, T. F. Rosenbaum, and G. Aeppli, Phys. Rev. Lett. **77**, 940 (1996).
[21] J. Brooke, D. Bitko, T. F. Rosenbaum, and G. Aeppli, Science **284**, 779 (1999).
[22] J. Brooke, Ph.D. thesis, University of Chicago, 2000.
[23] S. Ghosh, R. Parthasarathy, T. F. Rosenbaum, and G. Aeppli, Science **296**, 2195 (2002).
[24] S. Ghosh, T. F. Rosenbaum, G. Aeppli, and S. N. Coppersmith, Nature (London) **425**, 48 (2003).
[25] H. M. Rönnow, R. Parthasarathy, J. Jensen, G. Aeppli, T. F. Rosenbaum, and D. F. McMorrow, Science **308**, 389 (2005).
[26] H. M. Rönnow, J. Jensen, R. Parthasarathy, G. Aeppli, T. F. Rosenbaum, D. F. McMorrow, and C. Kraemer, Phys. Rev. B **75**, 054426 (2007).
[27] D. M. Silevitch, D. Bitko, J. Brooke, S. Ghosh, G. Aeppli, and T. F. Rosenbaum, Nature (London) **448**, 567 (2007).
[28] D. M. Silevitch, C. M. S. Gannarelli, A. J. Fisher, G. Aeppli, and T. F. Rosenbaum, Phys. Rev. Lett. **99**, 057203 (2007).
[29] P. E. Jönsson, R. Mathieu, W. Wernsdorfer, A. Tkachuk, and B. Barbara, Phys. Rev. Lett. **98**, 256403 (2007).
[30] C. Ancona-Torres, D. M. Silevitch, and T. F. Rosenbaum, Phys. Rev. Lett. **101**, 057201 (2008).
[31] P. E. Jönsson, R. Mathieu, W. Wernsdorfer, A. M. Tkachuk, and B. Barbara, arXiv:0803.1357 (unpublished).
[32] A recent experimental study suggest that there might not even be a spin-glass transition in $LiHo_xY_{1-x}F_4$ for $x\leq 0.16$, even in zero B_x. See Ref. 29 and the discussions in Refs. 30 and 31.
[33] M. Schechter and P. C. E. Stamp, Phys. Rev. Lett. **95**, 267208 (2005).
[34] M. Schechter and N. Laflorencie, Phys. Rev. Lett. **97**, 137204 (2006).
[35] S. M. A. Tabei, M. J. P. Gingras, Y.-J. Kao, P. Stasiak, and J.-Y. Fortin, Phys. Rev. Lett. **97**, 237203 (2006).
[36] J. A. Quilliam, C. G. A. Mugford, A. Gomez, S. W. Kycia, and J. B. Kycia, Phys. Rev. Lett. **98**, 037203 (2007).
[37] J. A. Quilliam, S. Meng, C. G. A. Mugford, and J. B. Kycia, Phys. Rev. Lett. **101**, 187204 (2008).
[38] Yet, an even more recent work argues, contrary to Refs. 24, 29, and 31, that a thermodynamic spin glass transition occurs in $LiHo_xY_{1=x}F_4$ for $x=0.045$. See Ref. 37.
[39] M. J. Stephen and A. Aharony, J. Phys. C **14**, 1665 (1981).
[40] J. Snider and C. C. Yu, Phys. Rev. B **72**, 214203 (2005).
[41] A. Biltmo and P. Henelius, Phys. Rev. B **76**, 054423 (2007).
[42] A. Biltmo and P. Henelius, Phys. Rev. B **78**, 054437 (2008).
[43] R. N. Bhatt and P. A. Lee, Phys. Rev. Lett. **48**, 344 (1982).
[44] A. Chin and P. R. Eastham, arXiv:cond-mat/0610544 (unpublished).
[45] K.-M. Tam and M. J. P. Gingras, arXiv:0810.0854 (unpublished).
[46] G. S. Shakurov, M. V. Vanyunin, B. Z. Malkin, B. Barbara, R. Y. Abdulsabirov, and S. L. Korableva, Appl. Magn. Reson. **28**, 251 (2005).
[47] S. Bertaina, B. Barbara, R. Giraud, B. Z. Malkin, M. V. Vanuynin, A. I. Pominov, A. L. Stolov, and A. M. Tkachuk, Phys. Rev. B **74**, 184421 (2006).
[48] N. I. Agladze, M. N. Popova, G. N. Zhizhin, V. J. Egorov, and M. A. Petrova, Phys. Rev. Lett. **66**, 477 (1991).
[49] J.-Y. Fortin and M. J. P. Gingras (unpublished).
[50] J. Magariño, J. Tuchendler, P. Beauvillain, and I. Laursen, Phys. Rev. B **21**, 18 (1980).
[51] Z. A. Kazei, V. V. Snegirev, R. I. Chanieva, R. Y. Abdulsabirov, and S. L. Korableva, Phys. Solid State **48**, 726 (2006).
[52] G. K. Liu, J. Huang, R. L. Cone, and B. Jacquier, Phys. Rev. B

38, 11061 (1988).
[53] G. Aeppli, in Proceedings of the NATO Advanced Study Institute on Dynamical Properties of Unconventional Magnetic Systems, edited by A. T. Skjeltorp and D. Sherrington (Kluwer, Dordrecht, 1998).
[54] In recent years, the frustrated ferromagnetic spin ice materials have attracted much interest (Ref. 78). These systems are extremely well described by a classical Ising model where the leading interactions are long-range magnetic dipole-dipole couplings in addition to a short-range exchange interaction (Ref. 79). The application of a magnetic field on these systems have been found to give rise to interesting effects (Ref. 80). There has also been studies of diluted spin ice compounds (Ref. 81). However, the excited crystal-field levels of so far considered $Dy_2Ti_2O_7$ and $Ho_2Ti_2O_7$ spin ice materials are at very high energy compared to typically accessible magnetic-field Zeeman energy (Ref. 82). As a result, field-induced quantum-mechanical fluctuation effects are negligible in spin ice materials (Ref. 80), and these are unfortunately not suitable materials for the purpose of exploring TFIM physics. One exception may be $Tb_2Ti_2O_7$ where, because of the smallest energy gap to the lowest excited doublet (Ref. 83) field-induced quantum effects may perhaps be investigated (Ref. 84).
[55] C. A. Catanese, A. T. Skjeltorp, H. E. Meissner, and W. P. Wolf, Phys. Rev. B **8**, 4223 (1973).
[56] P. D. Scott, Ph.D. thesis, Yale University, 1970.
[57] G. W. Beall, W. O. Milligan, and H. A. Wolcott, J. Inorg. Nucl. Chem. **39**, 65 (1977).
[58] G. H. Lander and T. O. Brun, Acta Crystallogr., Sect. A: Cryst. Phys., Diffr., Theor. Gen. Crystallogr. **29**, 684 (1973).
[59] P. D. Scott, H. E. Meissner, and H. M. Crosswhite, Phys. Lett. **28**, 489 (1969).
[60] H. G. Kahle, A. Kasten, P. D. Scott, and W. P. Wolf, J. Phys. C **19**, 4153 (1986).
[61] K. W. H. Stevens, Proc. Phys. Soc., London, Sect. A **65**, 209 (1952).
[62] M. T. Hutchings, *Point-Charge Calculations of Energy Levels of Magnetic Ions in Crystaline Electric Fields*, Solid State Physics Vol. 16 (Academic, New York, 1964), p. 227.
[63] By making this choice, we do not imply higher validity or better accuracy of the chosen sets of crystal-field parameters.
[64] P. D. Scott and W. P. Wolf, J. Appl. Phys. **40**, 1031 (1969).
[65] S. Karmakar, M. Saha, and D. Ghosh, J. Appl. Phys. **52**, 4156 (1981).
[66] S. Karmakar, M. Saha, and D. Ghosh, Phys. Rev. B **26**, 7023 (1982).
[67] C. A. Catanese and H. E. Meissner, Phys. Rev. B **8**, 2060 (1973).
[68] P. P. Ewald, Ann. Phys. **369**, 253 (1921).
[69] J. M. Ziman, *Principles of the Theory of Solids* (Cambridge University Press, Cambridge, 1972).
[70] S. W. de Leeuw, J. W. Perram, and E. R. Smith, Proc. R. Soc. London, Ser. A **373**, 27 (1980).
[71] M. Born and K. Huang, *Theory of Crystal Lattices* (Oxford University Press, London, 1968).
[72] R. G. Melko and M. J. P. Gingras, J. Phys.: Condens. Matter **16**, R1277 (2004).
[73] C. A. Catanese, Ph.D. thesis, Yale University, 1970.
[74] C. P. Tigges and W. P. Wolf, Phys. Rev. Lett. **58**, 2371 (1987).
[75] W. P. Wolf, Braz. J. Phys. **30**, 794 (2000).
[76] J. Jensen and A. R. Mackintosh, *Rare-Earth Magnetism Theory—Structures and Excitations* (Clarendon, Oxford, 1991).
[77] T. I. K. Deguchi and Y. Maeno, Rev. Sci. Instrum. **75**, 1188 (2004).
[78] S. T. Bramwell and M. J. P. Gingras, Science **294**, 1495 (2001).
[79] B. C. den Hertog and M. J. P. Gingras, Phys. Rev. Lett. **84**, 3430 (2000); T. Yavors'kii, T. Fennell, M. J. P. Gingras, and S. T. Bramwell, Phys. Rev. Lett. **101**, 037204 (2008);
[80] J. P. C. Ruff, R. G. Melko, and M. J. P. Gingras, Phys. Rev. Lett. **95**, 097202 (2005).
[81] X. Ke, R. S. Freitas, B. G. Ueland, G. C. Lau, M. L. Dahlberg, R. J. Cava, R. Moessner, and P. Schiffer, Phys. Rev. Lett. **99**, 137203 (2007).
[82] S. Rosenkranz, A. P. Ramirez, A. Hayashi, R. J. Cava, R. Siddhart, and B. S. Shastry, J. Appl. Phys. **87**, 5914 (2000).
[83] M. J. P. Gingras, B. C. den Hertog, M. Faucher, J. S. Gardner, L. J. Chang, B. D. Gaulin, N. P. Raju, and J. E. Greedan, Phys. Rev. B **62**, 6496 (2000); H. R. Molavian, M. J. P. Gingras, and B. Canals, Phys. Rev. Lett. **98**, 157204 (2007).
[84] K. C. Rule, J. P. C. Ruff, B. D. Gaulin, S. R. Dunsiger, J. S. Gardner, J. P. Clancy, M. J. Lewis, H. A. Dabkowska, I. Mirebeau, P. Manuel, Y. Qiu, and J. R. D. Copley, Phys. Rev. Lett. **96**, 177201 (2006); H. R. Molavian and M. J. P. Gingras, arXiv:0809.3477 (unpublished).